JPRS-CST-94-002
25 February 1994

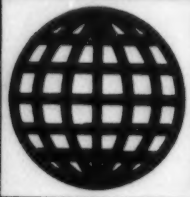

FOREIGN
BROADCAST
INFORMATION
SERVICE

JPRS Report

Science & Technology

China

Science & Technology
China

JPRS-CST-94-002 25 February 1994

CONTENTS

Caohejing New-Technologies Development Zone Update

94P60101A Beijing RENMIN RIBAO OVERSEAS EDITION in Chinese 15 Jan 94 p 1

[Article by Guo Changxi [6753 2490 3588], Zheng Xian [6774 2009], and Zhou Zhenbang [0719 2182 6721]: "Caohejing Development Zone Taking Shape"]

[Summary] Shanghai, 14 Jan (RENMIN RIBAO wire report)—The Shanghai Caohejing New-Technologies Development Zone over its five-year-plus history has become an export-oriented, multifunctional new high-tech industrial park that has attracted investment and related plant construction by a number of internationally known high-tech corporations. Aggregate gross investment for the 115 foreign-funded enterprises in the zone has reached US$600 million, while foreign capital attracted is at $360 million, of which there are 15 projects (about 14 percent of the 115) funded with at least $10 million each.

Within the Caohejing Zone, Shanghai Beiling Microelectronics Mfrg. Ltd., Shanghai Microelectronics Engineering Research Center, and Shanghai Philips Semiconductor Corp. have formed a technologically advanced microelectronics industry mini-zone integrating research, development, intermediate testing, production, and sales. This mini-zone has an industrial-grade, communications-grade, and consumer-grade large-scale integrated circuit (LSI) production capacity outfitted with 0.65-micron IC design technology, technology for producing 4-5-inch silicon wafers, and technology for fabricating 1.2-3-micron ICs. A Shanghai fiber optic communications industrial base has taken shape around the Shanghai Fiber Optic Communications Engineering Co., Shanghai AT&T Communications Equipment Ltd., and the Sino-U.S. joint venture AT&T Fiber Optic Communications Ltd. Some 30 firms, including Shanghai Foxboro Co. and Shanghai Qiming [0796 2494] Software Ltd., have formed a computer software industrial group engaged in R&D of products for industrial and office automation, information and enterprise management, finance, insurance, and commerce. The wholly U.S.-owned 3M China Ltd., the Sino-U.S. joint venture Shanghai Ruikan [3843 0170] (Electric) Cable Accessories Ltd., and the British firm ICI Co. have formed an international-state-of-the-art production base for industrial new materials. Finally, Caohejing has the nation's first bioengineering R&D/intermediate-testing base—the Chinese Academy of Sciences' (CAS) Shanghai Bioengineering Research Center and other Sino-foreign joint ventures have formed an embryonic bioengineering industrial development zone.

As of the end of 1993, the Caohejing Zone's industrial gross output value exceeded 4.2 billion yuan, business sales income exceeded 5.5 billion yuan, industrial profits approached 700 million yuan, annual per capita sales income for foreign-funded enterprises within the development zone reached 330,000 yuan, and annual per capita profit was 70,000 yuan.

Appetite Grows for Electronics

40100036A Beijing CHINA DAILY (BUSINESS WEEKLY) in English 14 Feb 94 p 1

[Article by Pei Jianfeng: "Appetite Grows for Electronics"]

[Text] China's exports—and imports—of electronics rose sharply last year.

According to statistics from the General Administration of Customs, exports of electronic products amounted to $8.1 billion in 1993, up 18.1 percent over 1992.

Imports, meanwhile, jumped 32 percent to $10.6 billion.

Imports of visual and audio merchandise and telecommunications products hit $5.53 billion, while exports totalled $5.01 billion.

About $3.62 billion of electronic components and instruments were imported and $1.51 billion worth were exported.

Foreign-funded enterprises are playing a bigger role in the exports, said a senior official from the Ministry of Electronics Industry.

Last year foreign-funded enterprises accounted for more than 40 percent of all exports. The proportion will continue to grow in the coming years, the official said.

Exports of consumer electronics kept rising last year. China exported 113 million cassette tape recorders worth $150 million and 11.31 million television sets of which 6.95 million were black and white.

China's exports of cassette tape recorders and black-and-white TV sets rank first in the world.

The official said China is trying to increase exports of electronic products for investment use and basic electronic components.

For example, China exported $558 million worth of computers and related products last year, an increase of 85 percent over 1992.

Last year's 18.1 percent growth in electronic exports actually was a slowdown from 1992, when they jumped by more than 40 percent over 1991.

The ministry official attributed the slower expansion to the brisk domestic market and exporters' shortage of capital.

According to the ministry's statistics for 1993, Chinese electronic production reached 139.8 billion yuan ($16 billion), an increase of 26.4 percent over 1992. Sales jumped by 37.6 percent to 113.27 billion yuan ($13 billion).

The official said China now mainly exports low-grade products, which yield low profits.

He noted that while exports of TV sets increased by 20 percent last year, their value rose by only 5 percent.

At present, China depends on Hong Kong and Macao to absorb its exports, but the official said other markets will be explored.

Although the imbalance in the trading of electronics accounted for nearly 20 percent of China's entire trade deficit last year, the ministry official said imports will probably continue growing rapidly this year.

This expanding market for electronics has drawn the attention of many foreign companies, which are eager to supply the up-to-date equipment China needs to modernize itself. For instance, the country plans to set up nationwide economic information networks that will need sophisticated technology from abroad.

Last year, many big names in the international industry sent high-profile delegations to China seeking business.

More are expected this year. Lou Gerstner, chairman of IBM Corp., the world's largest computer maker, and William H. Gates III, chairman of Microsoft Corp., the software giant, are scheduled to make their first visits to China separately in March.

Ministry of Electronics Industry Holds Expert Forum for Ninth FYP, 2010 Planning

94FE0261A Beijing ZHONGGUO DIANZI BAO [CHINA ELECTRONICS NEWS] in Chinese 17 Nov 93 pp 1-2

[Article by Liu Weili [0491 5898 7787]: "Ministry of Electronics Industry Organizes Expert Forum for Electronics Industry Development Planning"]

[Text] From 19 to 20 October 1993, the General Planning Department and the Technology and Quality Monitoring Department of the Ministry of Electronics Industry (MEI) held a joint expert forum in Beijing for the Ninth Five-Year Plan (FYP) and for 2010 planning. The forum was attended by experts and supervisors from more than 40 units in the ministerial system. MEI Deputy Minister Zhang Jinqiang [1728 0093 1730] gave an important speech at the forum. Also present were Director Wu Xiaolong [0702 1420 7893] and Deputy Directors Xu Shuncheng [1776 7311 2052] and Wang Jianzhang [3769 1696 4545] of the General Planning Department, Director Li Houbin [2621 0624 7001] of the Technology and Quality Monitoring Department, Director Li Dasheng [6786 1129 0581] of the Basic Product and Major Projects Department, and Deputy Director Chen Zhengqing [7115 2973 3237] of the Computer and Information Promotion Department.

Zhang Jinqiang analyzed in his speech recent achievements and existing problems of China's electronics industry. He emphasized conceptual planning for the Ninth FYP and 2010. He pointed out that plans for the Sixth, Seventh, and Eighth FYPs were all formulated under a planned economics system and carried a heavy planned-economy flavor. While planning for the Ninth FYP, we are faced with a very different setting. First, as the socialist market economy matures, the market is playing an increasingly stronger role in the allocation of resources. Second, when China joins GATT, the domestic market and the foreign market will merge to form a greater market. With these premises, we must be innovative conceptually and practically in our planning for the Ninth FYP. We must on the one hand learn from the previous FYPs and on the other hand seize the opportunity of the new reform situation in China and adjustment of the international electronics industrial structure. We should formulate a plan for the greater industry and the greater market. The plan should be authoritative and of a guiding nature. He stressed the following five major points:

(1) Strengthen macroscopic control and practice industry-wide management. The plan should be beyond departments and ownership. It should be an industry-wide plan for state-owned, collectively-owned, private, and foreign businesses.

(2) Implement the new "16-word" development strategy.

(3) Make fundamental changes in ideology, both in job function and in development approach.

(4) Lead the development with systems engineering and network engineering. Here he described in detail 20 major projects in the ministry.

(5) Pay attention to key products, key enterprises, and key regions.

Li Houbing described the main functions of the Technology and Quality Monitoring Department and progress in technical planning. He also analyzed the relationship between industrial planning and technology planning and the importance of technology to the advance of the electronics industry. Wu Xiaolong expressed three opinions. First, the main point of

planning is no longer how to divide the money and materials. With limited financial resources, the state resources must reside on major engineering projects. Second, we must properly handle the relationship between domestic and foreign issues and make full use of the "two resources, two markets." Joining GATT will place Chinese products on equal footing in competing with foreign products. We must therefore aim high and pay attention to economic efficiency. Third, we should avoid repetition.

The attending experts listened to the presentations of Zhang, Li and Wu and conducted wide-ranging discussions on communications, television broadcasting, computers and software, microelectronics, basic products and military applications. They made the following recommendations for the Ninth FYP and 2010:

I. Methods for Speeding Up Development

(1) New Understanding of the "16-Word" Strategy

We must first adhere to "market orientation" and organize our production and macroscopic control according to the market supply and demand. We must change the old practice of paying attention only to production and ignoring management, and centering all activities on the plan and not the market. In the meantime, we must use efficient industrial management to promote consumption and direct the market. Second, we should combine the strategy of "using the foreign market to stimulate the domestic market" and the development model of "using offense as a defense." We need to carry forward the development of some basic industries in China by exporting. For example, we can proceed to produce HDTV receivers that meet U.S. standards for the U.S. market and by so doing develop domestic HDTV receivers and related industries in China.

(2) Strengthening Industrial Management and Information Guidance

We should avoid duplication, improve industrial management, and include all enterprises, including village and city enterprises and "tri-investment" enterprises into the management system. To enhance management, MEI should implement several constraint and control measures. Examples are the right to formulate product and technical standards, and to certify equipment. They recommended a reform of the State Radio Regulatory Committee so that it may transcend other departments and become more efficient.

(3) Establishing China's Own Industry

The strength of the industry is in its products. There can be development only when the products meet the needs of the customers. We should make the development of the "Golden Card" a major business in China. If MEI itself is buying the "Golden Card" from foreign countries, then the banks can also buy it and there would be no need for MEI to develop it. China was practicing importing during the Sixth and Seventh FYPs and cooperation during the Eighth FYP; now it is time to establish our own industry and stop relying on others.

(4) People as the Key to Development

Much more attention should be given to people and stability of the ranks. In recent years people in enterprise units are flowing toward joint-venture and independently owned businesses, offices of foreign businesses in China, and toward the eastern coastal areas. This human flow has left many business units with technical staffs trained in the 1950s and 1960s. There is now an alarming discontinuity in human resources, which is extremely detrimental to the development of the electronics industry. The forum recommends that MEI perfect its reward system, formulate corresponding policies, and stabilize ranks. This has a direct impact on the realization of goals set for the Ninth FYP and 2010.

(5) Reconciling Research and Production

Speed up the reform of the old scientific research system, establish national high-tech venture capital foundations, let the state share the risks and benefits with the enterprises and the research institutes. Pay attention to basic research and technology reserves, provide protection via investment policy.

II. Development Trends for Ninth FYP and 2010

(1) Communications and Television

The trends in communications and television are digital technology, multi-media, software, and system networking. In the short term, analog mobile communications products will still be the lead product in the Chinese market, and we must quickly master the technology for mass production. For digital mobile communications products we need to excel in research and follow this technology. Fiber-optic communications will be centered on the development of synchronous fiber-optic technology. The main task in microwave communications is to improve the volume, quality, and reliability. Satellite communications will again be based on digitized transmission. Developments in television will include a CATV system based on fiber-optic transmission. Digital TV will be gradually commercialized and China needs to conduct research and technology tracking for [digital] HDTV.

(2) Computers and Software

The unification of computers and communication characterizes an information society. Parallel processing is an important way to improve computing and

will be the trend for future mid-size and main-frame computers. Software and information services are capturing a greater share in the computer industry. The triad of software, systems integration, and services is the main trend in software development. Multi-media will become practical. Magnetic recording will move toward greater volume and density and magneto-optical disks will find broad application in computers. Computer security will receive increasing attention. Software operating systems will be based on Unix and Windows. Software development should move toward public-domain applications and development tools should move from single to integrated. Development methods will go from the traditional methods toward object-oriented approaches.

The Ninth FYP should emphasize notebook computers. China has already made some progress in workstations and the efforts should continue. The software industry should stress application software, especially high-level software packages. The technology for software tools and systems software should be tracked.

(3) Microelectronics

The future development trends in microelectronics are integrable, programmable FPGA [field-programmable gate array] technology, MOSYS systems, hybrid ICs, and quantum devices. Development emphasis for the Ninth FYP should be placed on the following items: When introducing new technology for the low-grade or medium-grade products already on the market, the emphasis should be on the novelty and not on the high tech. Practice secondary integration using existing foreign technology and products. Strive for breakthroughs in the design of ICs. Pay attention to packaging and broaden the applications of microelectronics in the automobile industry.

(4) Basic Products

Production of components will continue to move toward miniaturization, thin-film usage, and large-scale integration. Mass-production technology will receive great attention. Emphasis in the Ninth FYP should be as follows: In component production, chip-type components are yielding the mid-grade market in favor of low-grade, high-consumption components and high-grade products with high added value. The development of sensors and transducers should stress silicon-on-sapphire [SOS] transducers with high stability in a high humidity environment, low-voltage pressure-sensitive resistors, and thin-film Hall devices. The emphasis in electronic components should be hybrid ICs, electronic power meters, electronic cards, and heat sensors. Electronic functional materials should stress sensing materials, precision electronics ceramics, high-density and low-noise magnetic recording materials, fiber-optic materials, high-energy-density rare earth permanent magnetic materials, and new types of acousto-optic materials. For relays and connectors, China should first develop relays and connectors used in communications and television, solid-state relays and chip connectors, ICs, and multi-layer printed circuit boards. Second, China should mass-produce black-and-white and color TFTs [thin-film transistor LCDs] and monochrome and black-and-white STN [supertwist-nematic LCDs] used in opto-electronics. Third, in the area of electronic equipment and special facilities, China should emphasize communications equipment and equipment for precision manufacturing.

(5) Military Electronics

Modern war has placed a higher demand on electronics technology. Experts at the forum made forecasts for the needs in China's command systems, navigation guidance systems, friend-or-foe identification systems, information systems, aerospace systems, and traffic control systems, and identified the key technologies for each system.

Method for Realizing Spaceborne SAR Digital Imaging

94FE0160A Beijing DIANZI XUEBAO [ACTA ELECTRONICA SINICA] in Chinese Vol 21 No 9, Sep 93 pp 55-58

[Article by Li Chunsheng [2621 2504 0581], Li Jingwen [2621 2529 2429], and Zhou Yinqing [0719 5593 3237] of the Dept. of Electronic Engineering, Beijing University of Aeronautics and Astronautics, Beijing 100083: "Method for Realizing Spaceborne SAR Digital Imaging"; MS received Feb 92, revised Nov 92]

[Text]

Abstract

In this paper, a method of high-resolution digital imaging using spaceborne synthetic aperture radar (SAR) is presented. Computer digital images are generated using raw radar data collected by the U.S. ocean surveillance satellite SEASAT-A. The images cover 2,048 cells in the range direction and two synthetic apertures in the azimuth direction with an imaging area of approximately 38 km x 34 km. The high-quality radar images with a resolution of 25 m x 25 m have demonstrated the effectiveness of the proposed method.

I. Introduction

During the past 20 years, the use of synthetic aperture radar (SAR) as an advanced microwave remote sensor has attracted a great deal of attention. Since the mid-1970s, SAR technology has evolved from airborne applications to spaceborne applications. In recent years, significant progress has been made in spaceborne SAR technology. Since the launch of the SEASAT-A satellite by the U.S. National Aeronautics and Space Administration in 1978, the U.S. SIR-A, SIR-B, SIR-C, and European ERS-1, the Canadian RADARSAT and the Japanese JERS-1 satellites have all been equipped with advanced SAR imaging systems.

The unique features of spaceborne SAR systems are: high altitude, extended range and coverage, wide bandwidth, and high data rate; also, various error correction and compensation schemes and complex signal processing techniques are used in spaceborne SAR. There are distinct differences between spaceborne SAR and airborne SAR. Because of the relatively low altitude and slow velocity of airborne SAR, the Earth can be regarded as a large planar surface, which makes signal processing relatively easy. In the case of spaceborne SAR, however, the effects of Earth rotation and Earth curvature produce coupling in the radar returns between the range direction and the azimuth direction; as a result, azimuth compression of the radar signal becomes very complicated. In general, digital image processing for spaceborne SAR involves range processing, azimuth processing, motion compensation and multi-look processing, of which the most difficult problems are azimuth processing and motion compensation. In this paper, a method of digital imaging using spaceborne SAR is presented. The effectiveness of this method is demonstrated by the high-resolution images generated using raw radar data collected by the U.S. SEASAT-A satellite.

II. Mathematical Model of the Radar Signal

The radar transmits a linear frequency-modulated (FM) pulse signal. Let Δ be the pulse width, T be the pulse repetition period, R(t) be the slant range between the satellite and the ground target, $W_a(t)$ be the azimuth directivity function of the antenna, $\sigma(x,r)$ be the scattering coefficient of the ground target, a(t) be a step function of width Δ, λ be the wavelength, and c be the speed of light; then the radar return signal can be expressed as:[1]

$$s(x,r) = \sigma(x,r)W_r(r) * h_1(x,r) *_r h_2(x,r) \qquad (1)$$

where $W_r(r)$ is the range directivity function of the antenna, * is the two-dimensional convolution with respect to azimuth x and range r; $*_r$ is the one-dimensional convolution with respect to range r. Also,

$$h_1(x,r) = W_a(x)\exp\left\{-j\frac{4\pi R(x)}{\lambda}\right\}\delta[r-R(x)] \qquad (2)$$

$$h_2(x,r) = \frac{2}{c\sigma}a(\tau)\exp\left\{-j\frac{4\pi b}{c^2}r^2\right\} \qquad (3)$$

$$R(x) = R(0)+\frac{\lambda}{2}\left[f_s\frac{x}{v}+\frac{1}{2}f_s\left(\frac{x}{v}\right)^2\right] \qquad (4)$$

In the above equation, f_D is the Doppler center frequency, f_R is the rate of change of Doppler frequency, v is the satellite velocity relative to the ground, and b is the frequency-modulation rate.

One can see from the radar signal model that the radar return is a complicated two-dimensional convolution; the purpose of signal processing is to extract the scattering characteristics of the target from the received signal, and ultimately to form a high-quality radar image.

III. Range-Compression Processing

Range processing of spaceborne SAR actually implies pulse compression. Digital pulse compression in the range direction uses FFT for matched filter implementation. The processed signal can be expressed as:

$$s_R(x,r) = s(x,r) *_r h_2^*(x,r)$$

$$= \sigma(x,r) * h_1(x,r) *_r \mathrm{sinc}\,c_0 r/c_0 r \qquad (5)$$

where $c_0 = 2\pi b\Delta/c$.

It is known from the principle of pulse compression that the slant range resolution after pulse compression is:

$$\rho_r = c/2B_r$$

and the ground range resolution is:

$$\rho_{rg} = \rho_r \left(\frac{H+R_e}{R_e} \cdot \sin\theta\right)^{-1} \qquad (6)$$

where B_r is the signal bandwidth, H is the satellite altitude, R_e is the mean Earth radius, and θ is the antenna viewing angle. The number of samples of the range reference function is

$$N_r = \Delta \cdot f_s$$

where f_s is the sampling frequency.

The raw data collected by SEASAT-A are digital data produced by the A/D converter; prior to range processing, they must first be orthogonalized and then matched-filtered. The orthogonalization process is accomplished in the frequency domain, where a window function is applied and the signal carrier frequency is shifted to zero frequency; finally, a complex IFFT [inverse fast Fourier transform] is performed to complete the process of range digital pulse compression. This process is equivalent to a transformation from real data to complex data; the complex data are stored for azimuth processing.

IV. Azimuth-Compression Processing

The azimuth reference function is chosen based on the expression of the range-compressed radar signal:[2]

$$h_a(x,r) = W_a(x)\frac{\mathrm{sinc}_0[r-R(x)]}{c_0[r-R(x)]}\exp\left\{-j\frac{4\pi R(x)}{\lambda}\right\} \qquad (7)$$

Due to the effect of range drift, coupling between the range direction and the azimuth direction exists in the radar return; therefore, azimuth processing requires complicated two-dimensional processing. In fact, azimuth processing is actually a two-dimensional matched filtering; the filtered output signal represents the scattering characteristics of the ground target, which is of the form:

$$\sigma_0(x,r) = s_R(x,r) * h^*_a(x,r) \qquad (8)$$

The implementation of two-dimensional matched filtering for azimuth processing is highly computation-intensive. By using a hybrid time-domain and frequency-domain correlation technique, the two-dimensional problem reduces to a one-dimensional problem, and the correction of range drift can be accomplished in the frequency domain; as a result, the amount of computation is greatly reduced. For a second-order curve R(x), the azimuth reference function for range r_0 is:

$$h_1(x,r,r_0) = = \sum_{i=1}^{N} g_i(x,r_0)\delta(r-d_i) \qquad (9)$$

where d_i is the distance of the range reference value r_0, and

$$g_i(x,r_0) = W_a(x)\frac{\mathrm{sinc}_0[r_0-R(x)]}{c_0[r_0-R(x)]}\exp\left\{-j\frac{4\pi R(x)}{\lambda}\right\} \qquad (10)$$

The expression in the frequency domain after azimuth processing is of the form:

$$Q(\omega,r_0) = \sum_{i=1}^{N} S_R(\omega,d_i+r_0)G_i^*(\omega,r_0) \qquad (11)$$

It can be seen from the above expression that the hybrid correlation method uses time-domain correlation in the range direction and frequency-domain correlation in the azimuth direction; this approach takes full advantage of the FFT and therefore provides an efficient way of calculating precision impulse response.

If the above method is applied directly for azimuth compression, the amount of computation will increase with increasing Doppler center frequency. A more efficient way would be to apply correction to the range wander (the linear term of range drift) before azimuth pulse compression, then apply correction to the range bending (the second-order term of range drift) in the frequency domain; this approach requires less computation, and R(x) in the azimuth reference function $g_i(x,r_0)$ becomes:

$$R(x) = R(0) + \frac{\lambda}{4}f_R\left(\frac{x}{v}\right)^2 \qquad (12)$$

Computer results show that the digital images of spaceborne SAR produced by this method and the previous method are almost identical, but the amount of computation for azimuth compression (at f_D = 980 Hz) is reduced by one half.

V. Motion Compensation

Because of antenna pointing error and errors caused by satellite motion, it is difficult to accurately estimate the Doppler center frequency and the rate of change of Doppler frequency from satellite historical data and from SAR parameters. Inaccuracy in the Doppler center frequency and in the rate of change of Doppler frequency will have an adverse effect on SAR images. Inaccuracy in the Doppler center frequency will result

in lower signal-to-noise ratio, which in turn will cause an increase in the fuzziness in azimuth and a shift in the target position. Inaccuracy in the rate of change of Doppler frequency will cause defocusing in the radar images and result in a decrease in pixel resolution. An effective method of estimating the Doppler parameters is to estimate the errors in the Doppler parameters directly from the radar return data.

The clutter lock used for estimating the errors in the Doppler center frequency is obtained from the normalized energy difference of the symmetric multi-look sub-images.[3] Experimental results show that the error in the Doppler center frequency is proportional to the normalized energy difference ΔE:

$$\Delta f_D \approx f_R T \Delta E \qquad (13)$$

where T is the time required for the satellite to travel the distance of one aperture.

The auto-focusing used for estimating the rate of change of Doppler frequency is determined by the relationships between the multi-look sub-images. The offset between the first-look sub-image and the Nth-look sub-image ΔX can be obtained from the relationship between the two sub-images. Experimental results show that the offset is proportional to the errors in the rate of change of Doppler frequency:

$$\Delta f_R \approx f_R \Delta X / vT \qquad (14)$$

Accurate estimates of the Doppler center frequency and the rate of change of Doppler frequency can be obtained by an iterative procedure. For example, for an image around the city of London, the estimation error of the Doppler center frequency is less than 10 Hz, and the estimation error of the rate of change of Doppler frequency is less than 0.3 Hz/sec.

VI. Spaceborne SAR Digital Imaging

Raw radar data of an area around the city of London have been collected by the U.S. SEASAT-A satellite; the center of the area is located at 51.43° N. latitude and 0.33° E. longitude. The radar parameters and signal processing parameters are as follows:

Sampling frequency	45.53 MHz
Sampling width	300.5 μs
Quantization accuracy	5 bits
Wavelength	0.235 m
Modulation frequency	11.38 MHz
Pulse repetition frequency	1647 Hz
Pulse width	33.9 μs
Signal bandwidth	19.0 MHz
Average satellite height	800 km
Antenna viewing angle	20°

The estimated Doppler center frequency and the rate of change of Doppler frequency are approximately 940 Hz and 505 Hz/s, and the range drift is 43 range resolution cells. In order to reduce the effect of spot noise during the formation of the radar signal, we use an iterative procedure of non-coherent integration of 4-look sub-images. Figure 1 [photo not reproduced] shows the computer-generated digital image obtained using the method given in this paper. The processed image has a resolution of 25 m x 25 m; the imaging area covers 2,048 range cells and two synthetic apertures in the azimuth direction, which corresponds to an area of approximately 38 km x 34 km. During the imaging process, Doppler parameters are estimated every 128 range cells.

VII. Conclusion

By applying the spaceborne SAR digital imaging method presented in this paper, we have generated computer images using raw radar data collected by the U.S. SEASAT-A satellite. These are the first high-resolution spaceborne SAR images obtained in this country; the image resolution is 25 m x 25 m. The results of computer images have verified the effectiveness of the proposed method.

References

1. Li Chunsheng, Li Jingwen, and Zhou Yinqing, "Spaceborne Synthetic Aperture Radar Image Processing," ACTA ELECTRONICA SINICA, 1991, 19(1): 20-24.
2. Chialin, K. Y. Liu, and Michiel Jin, "Modeling and a Correlation Algorithm for Spaceborne SAR Signals," IEEE TRANS., September 1982, Vol AES-18(5).
3. F. K. Li, D. N. Held, and J. Curlander, "Doppler Parameter Estimation for Spaceborne Synthetic-Aperture Radars," IEEE TRANS., January 1985 on GEOSCIENCE AND REMOTE SENSING, Vol GE-23(1).

High Reynolds Number Wind Tunnel Completed

94FE0200A Beijing ZHONGGUO KEXUE BAO [CHINESE SCIENCE NEWS] in Chinese 12 Nov 93 p 1

[Article by Bu Xiangqun [0592 0686 5028]]

[Text] Beijing (CSN)—Construction of China's first high Reynolds number transonic two-dimensional wind tunnel at the Institute of Mechanics, Chinese Academy of Sciences (CAS) has been completed; on 30 October, it was certified by the CAS. The 14 members of the certification committee, which include renowned Chinese aerodynamicists, academic committee members, chief engineer of the China Aerospace Industrial Corp., Prof. Zhuan Fenggan, Prof. Dai Changhui, Prof. Lin Yunpei, and other experts believe

that the high Reynolds number transonic wind tunnel developed by the Institute of Mechanics matches leading wind tunnels of the world in terms of technical standard and performance.

The key simulation parameters in an aerodynamic test are the flight Mach number and Reynolds number. A conventional transonic wind tunnel can usually simulate the proper Mach number, but the simulated Reynolds number is typically one or two orders of magnitude lower than actual flight values. Therefore, some of the aircraft designed in the 1960s based on data obtained from conventional transonic wind tunnels developed problems. In an effort to avoid these problems, the United States, Canada, Europe, and Japan have invested huge sums of money since the 1970s to develop and construct high Reynolds number wind tunnels.

In the early 1980s, having developed an impulse type aerodynamic test facility and corresponding experimental techniques, experts of the Institute of Mechanics proposed the idea of building a high Reynolds number tubular wind tunnel; the initial design effort was led by Prof. Zhuan Fenggan. In 1988, the project was approved by the CAS.

With limited funds, members of the research and development group were determined to make this project a success. During the construction, they found innovative approaches that were compatible with China's limited industrial and economic resources, and succeeded in building the wind tunnel with a small investment and very short development cycle. The overall design has also built-in provisions for further improving the performance and expanding the utility of the wind tunnel. The success of this project has paved the way for future development of high Reynolds number transonic wind tunnels in China.

Antistatic Film's Performance, Its Application to Satellites

40100031A Beijing KONGJIAN KEXUE XUEBAO [CHINESE JOURNAL OF SPACE SCIENCE] in Chinese Vol 13 No 4, Oct 93 pp 286-291

[English abstract of article by Lu Yu-sun, Li Hua, and Cai Cun of the Lanzhou Institute of Physics, Chinese Academy of Space Technology, 730000; MS received 24 Nov 92]

[Text] Measured results of the electric and optical performance of ITO, IO and TO films are given. These films are prepared on substrates of flexible Kapton, Mylar and FEP Teflon by magnetron sputtering. Tests indicate that their stabilities under various conditions are quite good. The conductivity of the antistatic films in the simulated substorm environment is also measured. The results show that the modified flexible SSM can eliminate the charge accumulation on their surfaces and control the surface voltage below 80 Volts. On the contrary, the potential on the uncoated SSM surface can have a value up to 8-10 kV.

Effects of Space Particle Radiation on Integrated Chips in Satellite

40100031B Beijing KONGJIAN KEXUE XUEBAO [CHINESE JOURNAL OF SPACE SCIENCE] in Chinese Vol 13 No 4, Oct 93 pp 292-298

[English abstract of article by Pu Jian and Ye Zong-hai of the Center for Space Science and Applied Research, CAS, Beijing 100080; MS received 18 Feb 93]

[Text] The energy deposits in critical volumes of integrated chips produced by some radiated particles in Feng Yun-1 (B) satellite environment are analyzed. This is called linear energy translation (LET). We have obtained the LET of Galactic Cosmic-Ray components $1 \leq Z \leq 28$, Galactic Cosmic-Ray anomaly components (C, N, O, Ne, Ar, Fe), and inner radiation-belt protons. And single-event upset (SEU) ratios produced by these particles are calculated, respectively.

More Reports on Nanomaterials

Preparation, Optical Properties of Cu_2O Nanocrystals

94FE0161A Beijing KEXUE TONGBAO [CHINESE SCIENCE BULLETIN] in Chinese Vol 38 No 18, 16-30 Sep 93 pp 1649-1651

[Article by Zou Bingsuo [6760 3521 6956], Tang Gouqing [3282 0948 1987], Zhang Guilan [1728 2710 5695], and Chen Wenju [7115 2429 7467] of the Institute of Modern Optics, Nankai University, Tianjin, 300071, and Li Tiejin [2621 6993 3160], Zhang Yan [1728 1484], and Xiao Liangzhi [5135 5328 6347] of the Department of Chemistry, Jilin University, Changchun, 130023: "Preparation and Optical Properties of Cu_2O Nanoparticles," funded by the Natural Science Foundation of China and the Post-Doctoral Foundation of the State Education Commission; MS received 5 Nov 92, revised 1 Mar 93]

[Text] Key words: Cuprous oxide, nanoscale particles, preparation, exciton limitation, optical characteristics.

Due to the quantum confinement effect, semiconducting nanoparticles produce a series of new phenomena,[1,2] among which the materials with ultrafast optical nonlinear response have been particularly noticed. It is predicted that these semiconducting materials will be the basic optoelectronic materials of the future. The study of the opto-absorption and -relaxation properties of nanoscale crystals will help us further understand the mechanism of nonlinear optical response.

When the size of a semiconducting nanocrystal is as small as the Bohr radius a_B of its own phase, a series of changes of electronic state and optical property can be observed. These phenomena are observed in the semiconducting nanocrystal systems of CdS, CuCl, CdSe, PbS.[3,4] The ratio of the nanocrystal radius R to its Bohr radius a_B can be used as the general guideline to determine the influence of the quantum confinement effect on the electronic state:[5] When $R/a_B << 1$, the nanoparticles are in the strong quantum confinement zone, and their energy levels of electrons and holes are clearly separated; however, when $R/a_B >> 1$, the nanocrystal is in the exciton confinement zone where the excitons act as quasi-particles whose translation kinetic energy's degree of freedom is confined within the three-dimensional space; as a result the exciton energy increase is limited. Currently, only CuCl nanocrystals are being researched as an exciton-confinement-zone material, and they are also good model materials for the study of excitonic molecule properties. This paper presents the preparation of cuprous oxide (Cu_2O) nanocrystals and discussion of their optical properties, as well as a discussion of results based on the model of exciton responses to the quantum confinement effect.

1. Experiment

The Cu_2O nanocrystals are made by the oxidation-reduction method in a micro-emulsive liquid. The process flow diagram is as follows:

The Cu_2O nanocrystals made by this method are all coated with sodium dodecylbenzene sulfonate (DBS) molecules, and form a transparent sol with toluene. The crystal sizes can vary within the limit of 5-10.0 nm as determined by the initial value of $[CuAc_2]/[DBS]$. The transmission electron microscope and the low-angle X-ray scattering experiments show that the spread of the Cu_2O nanocrystal dimensions is very narrow. About 93 percent of the crystal dimensions have the median radius, and the rest are distributed within the 10 percent of the median radius. The radius distribution of the nanocrystals is thus well suited for the study of optical properties.

The room-temperature photoluminescence and excitation spectra of the Cu_2O nanocrystal sol series are measured with a Hitachi F-4000 fluorescence spectrometer.

2. Results and Discussions

The visible-ultraviolet absorption spectra of Cu_2O nanocrystal (9.0 nm) organic sol starts at 650 nm. The absorption rate gradually increases toward the high-frequency region, but there is no clear indication of

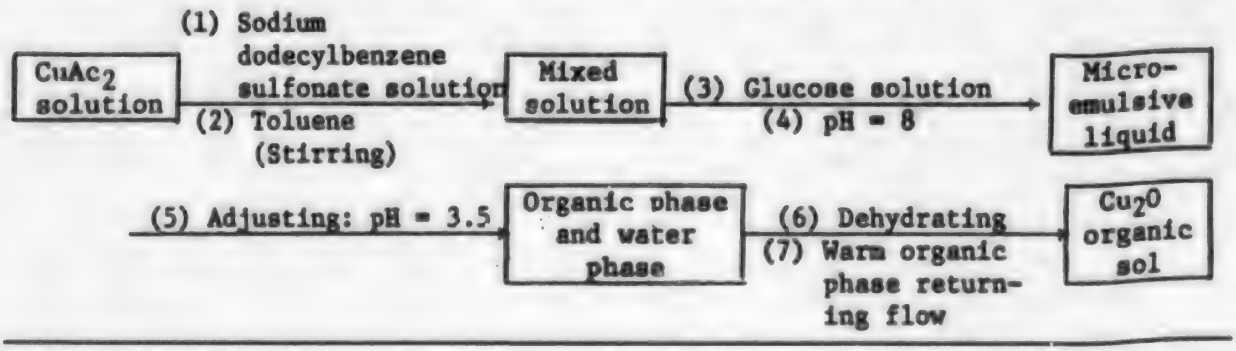

structural absorption characteristics. This implies that the phenomenon is influenced by two factors: one is the temperature and solvent effects; and the other is the size effect. Because the dimensions of the nanocrystal are far greater than the Bohr radius a_B (0.7 nm) of its own phase, the increase of the exciton energy is not obvious, and the energy separation induced by the confinement effect is very minor.

Figure 1 shows the photoluminescence spectra of the Cu_2O nanocrystals. The excitation luminescences are (1) 330 nm, (2) 400 nm, (3) 440 nm, (4) 460 nm, (5) 510 nm, and (6) 532 nm. Five luminescence bands are visible in the neighborhood of 400 nm, 475 nm, 505 nm, 540 nm and 565 nm. The last four bands correspond to the existing four luminescence bands in the exciton systems, namely, indigo, blue, green, and yellow.[6] The energy changes in the exciton confinement zone are comparatively small. The luminescences are undoubtedly fluorescence resonance emissions. In addition, the luminescence at 400 nm indicates the presence of energy jumps between bands within the Cu_2O crystal. The emission luminescence has not been reported in the past, but its absorption structure was reported long ago.[7] The emission from the bottom of the conduction band in the exciton confinement zone possibly originates from the bound excitons formed at the bottom of the band; however, further proof is needed. As to the luminescence phenomenon of solids at high energy level (or energy band), it is rarely seen in solid-state phases and many other nanocrystals. However, in our research we have observed that the phenomenon of increasing high energy-level radiation jumps not only takes place in the aforementioned Cu_2O nanocrystals, but could also occur in the coated CdS and PbS nanocrystals. It is quite likely that in the high energy-level neighborhoods of the quantum confinement and dielectric confinement zones, stable bound excitons are formed, and consequently, they reduce the non-radiation jumping probability of the electrons or holes due to vibrations or impurities; thus, they enhance the radiation jumping. The phenomenon deserves further probing, because it has direct bearing on the enhancement of the system's nonlinear optical phenomena.

Figure 2 shows the excitation spectra of Cu_2O nanocrystal (0.9 nm) emission at (a) 600 nm and (b) 580 nm. They are equivalent to the exciton wavelength absorption structure.[8] Figure 2 shows the exciton jumps in the indigo, blue, green, and yellow series are all mutually related,[6] and have an obvious relationship with the jump at about 380 nm. There is a corresponding spectral region of each individual series, and occasionally these spectral regions overlap. The relatively low vibrator absorption intensities of the yellow and green exciton series are caused by the dipole forbiddenness of the jump.[9]

Figure 1. Photoluminescence Spectrum of Cu_2O Nanocrystal (9.9 nm) Sol

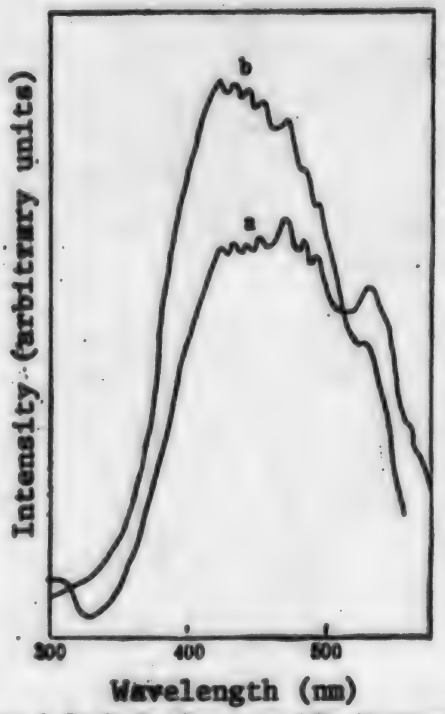

Figure 2. Excitation Spectrum of Cu_2 Nanocrystal (9.0 nm) Sol

a. 600 nm emission; b. 580 nm emission

Another interesting phenomenon in the excitation spectra is that the dipoles allow the indigo and blue exciton series having the multi-peak structures of jumps. Such structures are caused by the quantization of the exciton energy which in turn is due to the spatial quantum confinement effect.[10] Hanamura[2] has suggested a simplified mode. He assumes the exciton to be a quasi-particle situated in a semiconducting nanosphere; when $R/a_B >> 1$, the exciton energy ($l = m = 0$) that allows jumps is expressed as

$$E_n = E_0 - E^b_{ex} + n^2E_c \qquad (1)$$

where E_c is the quantum confinement energy ($h^2\pi^2/2\ M\ R^2$) and E^b_{ex} is the exciton bonding energy which varies with exciton's principal quantum number. The quantization of excitons follows the equation $E^b_{ex} = E_x/n^2$, where E_x is the effective exciton Rydberg energy ($\mu e^4/2h^2\varepsilon^2_0$), $M = m_e + m_h$, $\mu = m_e m_h/m_e + m_h$, and hence the equation

$$E_n = E_0 - E_x/n^2 + n^2E_c \qquad (2)$$

is used to describe the different exciton jumps with different principal quantum numbers in the same series. Our test results as shown in Figure 2 and Table 1 have proved the validity of Equation (2).

Table 1. Theoretical Value and Experimental Values of Indigo Exciton Jump

Experimental value (R = 4.5 nm, a_B = 0.7 nm)	Calculated value (R = 4.35 nm, E_C = 146,413 nm, E_X = 12,407 nm)
E_1 = 468.2	468
E_2 = 451	451
E_3 = 438	441.9
E_4 = 428.8	432.1
E_5 = 420.6	420.6

The aforementioned results demonstrate that the conclusion that the exciton energy increase in the exciton confinement zone is limited is valid only for the energy jump when $n = 1$. When $n \geq 2$, the blue shift of the jump is relatively significant. In this case, exciton jumps of different principal quantum numbers split away from one another, while the nanocrystal optical nonlinear response produces mesoscopic strengthening.[2] This phenomenon will benefit our study of mutual reactions among the excitons within the exciton confinement zone, such as the superradiation phenomenon.[1],[11] Thorough research on the above phenomenon would be very worthwhile.

Acknowledgment: The authors are grateful to Professor Zhang Guangyin for his valuable papers and beneficial discussions.

1) Zou Bingsuo, Ph. D. Thesis, Jilin University, 1991.

References

1. Brus, L. E., APPL. PHYS., A, 1991, 53: 465-474.
2. Hananura, E., PHYS. REV., B, 1987, 37: 1273-1278.
3. Li Shoutian, et al., GAODENG XUEXIAO HUAXUE XUEBAO [HIGHER EDUCATION CHEMICAL JOURNAL], 1991, 12: 1393-1395 [in Chinese].
4. Kayanuma, Y., et al., APPL. PHYS., A, 1991, 53: 475-479.
5. Efros, Al. L., et al., SOV. PHYS. SEMICOND., 1982, 16: 772-774.
6. Hanamura, E., "Excitonic Processes in Solids," Springer-Verlag, Berlin, 1986, 46-47.
7. Zhang Guangyin, et al., WULI XUEBAO [ACTA PHYSICA SINICA], 19[illegible], 21: 324-328 [in Chinese].
8. Kang, K. I., et al., PHYS. REV., B, 1992, 45: 3465-3468.
9. Agekyan, U. T., PHYS. STAT. SOL., (a), 1977, 43: 11-29.
10. Kayanuma, Y., PHYS. REV., B, 1988, 38: 9797-9805.
11. Itoh, T., et al., NONLIN. OPT., 1991, 1: 61-69.

Preparation of β-SiC Ultrafine Powder From Polysilane by CVD

93FE0226A Beijing GUISUANYAN XUEBAO [JOURNAL OF THE CHINESE CERAMICS SOCIETY] in Chinese Vol 21 No 5, Oct 93 pp 466-470

[Article by Zhang Changrui [1728 7022 3843] (correspondent), Chen Zhaohui [7115 2600 6540], Yan Dong [0917 0392], Song Yongcai [1345 3057 2088], and Chen Ge [7155 7245] of the Department of Materials and Applied Chemistry, National University of Defense Technology, Changsha, 410073: "Preparation of β-SiC Ultrafine Powder From Low-Molecular Polysilane by CVD"; MS received 12 Dec 91]

[Text]

Abstract

SiC ultrafine powder is prepared by the CVD [chemical vapor deposition] method using low-molecular polysilane as precursor and argon as carrying gas. The relationships between the powder properties and the preparation factors such as reaction temperature, carrying-gas flow rate, and reactant densities are studied. The β-SiC ultrafine powder with uniform size (< 0.1 μm), high purity (30 weight percent of carbon content),

and homogeneous crystalline structure is obtained through the decarbonization, deoxidization, and crystallization processes.

Key words: ultrafine silicon-carbide powder, CVD, low-molecular polysilane.

1. Introduction

Due to its high-temperature mechanical properties, and good thermal shock-resistance property, SiC is one of the major materials in research on using high-temperature ceramics for engine parts.[1]

To make superior ceramics by a sintering method, one of the crucial techniques is to prepare ultrafine (nano-scale) ceramic powders having the properties of non-agglomeration, size uniformity, and high purity.[2] The best method to prepare SiC ultrafine powder is the chemical vapor deposition (CVD) method.[3]

Among the several CVD methods, one is to prepare the SiC ultrafine powder from reactions between silicon-content monomers (e.g., $SiCl_4$, SiH_4) and carbon-content monomers (e.g., CH_4, C_2H_6),[4]; and another, from the thermal decomposition of organic silicon compounds containing both carbon and silicon (e.g., CH_3SiCl_3, CH_3SiH_3, $[(CH_3)_2Si]_2$, etc.).[2,5] However, in the monomer reactions, the existence of chlorine reduces the production rate, corrodes the equipment, and pollutes the environment. Moreover, when the carbon-to-silicon ratio (C/Si) is too low, too much free silicon is produced. Therefore, it is worthwhile to research other systems.

This paper studies the production factors of making SiC ultrafine powder from low-molecular polysilane (LPS), which is a by-product from synthesizing polyalkyl silane, as raw material and high-purity argon as carrying gas. The research also analyzes the composition, structure, and configuration of the ultrafine powder.

2. Experimental Work

2.1 Raw Materials: LPS is a by-product generated from the cracking process of making polyalkyl silane from polysilane. It is a pale yellow liquid composed of organic silicon oligomers with different boiling points. These oligomers have chain or ring structures with

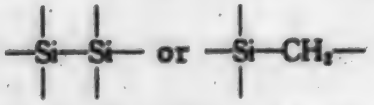

as the backbones, and an average molecular weight of 250. They vaporize completely at 300°C.

2.2 Carrying Gas: The carrying gas is high-purity argon with 12×10^{-6} of oxygen and 16.5×10^{-6} of H_2O as analyzed with a DH-3C trace-oxygen analyzer and a US-1-1A trace-water analyzer, respectively.

2.3 Apparatus for Preparation of SiC Ultrafine Powder: As shown in Figure 1.

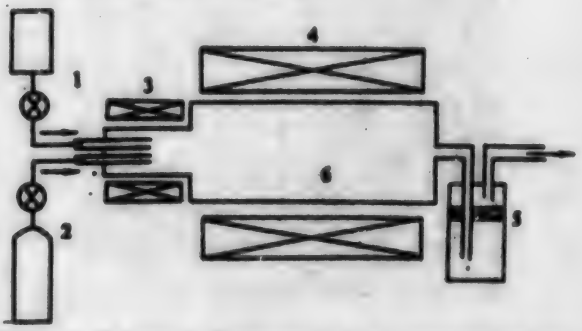

Figure 1. Schematic Diagram of the Apparatus for Preparation of SiC Ultrafine Powder

1. LPS and flowmeter; 2. Carrying gas and flowmeter; 3. Vaporizer; 4. Furnace; 5. Powder collector; 6. Pyrolysis tube

2.4 Decarbonization, Deoxidization and Crystallization of the Ultrafine Powder: The SiC ultrafine-powder product from the reaction is amorphous. The powder is treated at 1600°C for crystallization as well as decarbonization and deoxidization to remove the free carbon and oxygen in the ultrafine powder.

2.5 Ultrafine Powder Characteristics: The powder's infrared spectrum is obtained with a Hitachi 270-30 infrared spectrometer. The size and configuration of the powder are determined with a Hitachi H-800 transmission electron microscope (TEM); the powder crystal structure, with a type D/max-IIIA X-ray diffractometer; and the carbon, hydrogen, and nitrogen contents, with a USA PE2400CHN element analyzer.

3. Results and Discussions

3.1 Effects of Reaction Temperature

Under the condition that the argon flow rate is controlled at 0.24 L/min; and LPS flow rate, 0.025 g/min, different powder batches are made within the temperature range of 900 to 1300°C, as shown in the TEM photos in Figure 2. The reaction temperature has little effect on the particle size and configuration. The powder diameters are between 0.05 and 0.1 μm with very narrow distribution, and most particles are spherical.

(a) T_m =900℃

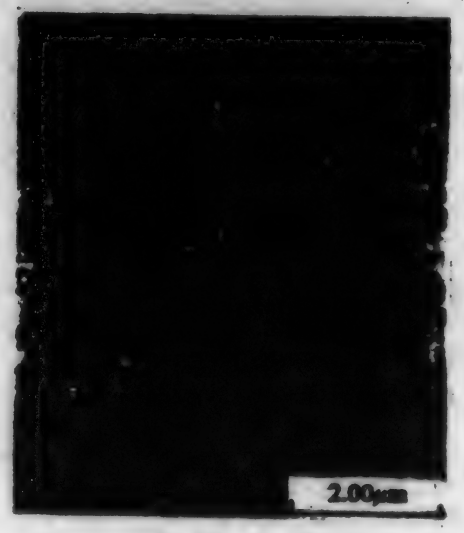

(b) T_m =1300℃

Figure 2. SEM Photographs of SiC Powder Synthesized at Different Temperatures

Ar: 0.24 L/min; LPS: 0.025 g/min; Vaporizer temperature: 200℃

Figure 3 shows the relationship between the powder's carbon and the hydrogen contents and the reaction temperature. The carbon content increases and the hydrogen content decreases with the increase of the reaction temperature. The fact that the hydrogen content in the SiC product is zero at the reaction temperature 1300℃ indicates that the transformation of the organic LPS to the inorganic SiC is complete. In LPS, the ratio of carbon to silicon is 2:1, therefore the total carbon content in the ultrafine powder exceeds the theoretical value (30 weight percent) and free carbon exists in the final product. At low temperature, the main cracking product is CH_4 which will be carried out by the gas flow; as a result, the carbon content is comparatively low for the low-temperature reaction product. At high temperature, the cracking product is mainly H_2, therefore the free-carbon content in the product increases.

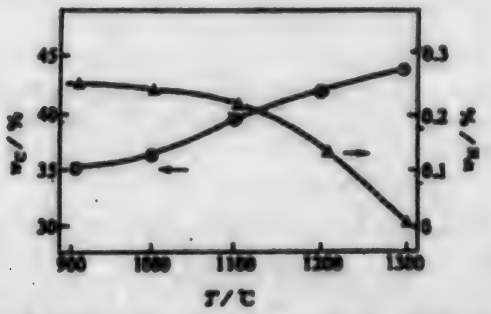

Figure 3. Effect of Reaction Temperature on the C and H Mass Content in SiC Powder

Figure 4 depicts the infrared spectra of products obtained at different temperatures. It shows that as the temperature increases, the transformation of the organic LPS to the inorganic SiC is gradually completed. At 450 cm^{-1}, there is a Si-O absorption peak. As the temperature increases, the peak becomes weaker. The existence of the Si-O bond is caused by the infusion of oxygen, one of the impurities in LPS.

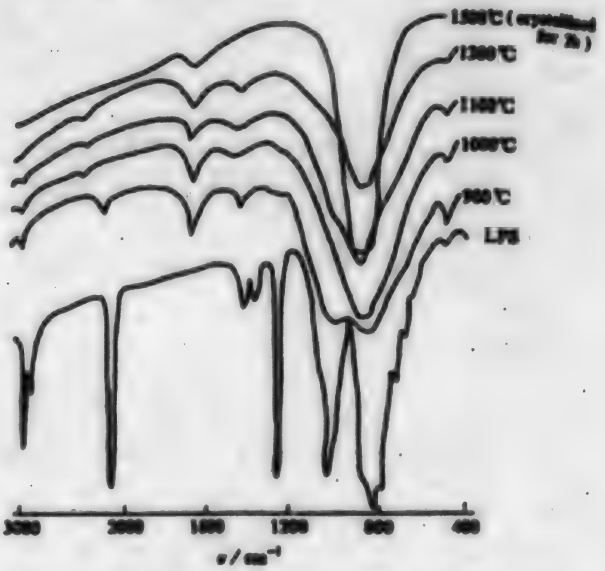

Figure 4. Infrared Spectra of LPS and Its Pyrolytic Products Obtained at Different Reaction Temperatures

3.2 Effects of Carrying-Gas Flow Rate

When the reaction temperature is controlled at 1100℃ and LPS flow rate at 0.025 g/min, at different argon flow

rates, the ultrafine powders remain spherical. When the argon flow rates are 0.088 L/min, 0.24 L/min, and 0.535 L/min, the diameters of the ultrafine powder are 0.1 μm, 0.075 μm, and 0.04 μm, respectively. The SiC ultrafine-powder diameter decreases with an increase in the argon flow rate. The SiC ultrafine-powder growth is a kinetics phenomenon. After SiC ultrafine powder is formed, its growth depends on its length of stay in the furnace. The higher the carrying-gas flow rate, the shorter the SiC's stay in the furnace, consequently the finer the powder produced.

3.3 Effects of LPS Flow Rate

When the furnace temperature is controlled at 1100°C and argon flow rate at 0.24 L/min, SiC ultrafine powders are prepared at different LPS flow rates. The results show that when the LPS flow rate is at 0.025, 0.065, or 0.160 g/min, all powders are spherical having a diameter 0.75 μm, which indicates that the LPS flow rate does not affect the size or the configuration of the SiC ultrafine powder.

3.4 Decarbonization, Deoxidization, and Crystallization of SiC Ultrafine Powder

As aforementioned, the SiC ultrafine powder prepared by this method contains free carbon and SiO_2, which as impurities produce unfavorable effects on the material; thus, decarbonization and deoxidization are needed. Besides, the prepared SiC ultrafine powder is amorphous, therefore, crystallization is also needed.

To achieve the purpose of decarbonization and deoxidization and in the meantime crystallization, this process utilizes high-temperature (about 1500°C) reaction in which free carbon reduces SiO_2 and forms gaseous SiO and CO, which eventually evaporate. At the same time the crystallization is also completed. The XRD results (Figure 5) show that as the crystallization temperature increases, the SiC ultrafine powder gradually transforms from the amorphous state to the β-SiC crystalline state. When the reaction temperature reaches 1500°C, β-SiC is virtually completely crystallized, and no other phases are observed.

Figure 4 shows that after crystallization for 2 hours at 1500°C, the infrared absorption peak at 450 cm^{-1} in the SiC ultrafine-powder spectrum disappears, which indicates that the powder is deoxidized.

The element analysis shows that the carbon content of decarbonized SiC drops from 39.54 percent to 30.15 percent, which is basically close to the theoretical carbon content (30 percent) of SiC. The fact that the color of the ultrafine powder changes from brownish to whitish also indicates that the powder is completely decarbonized.

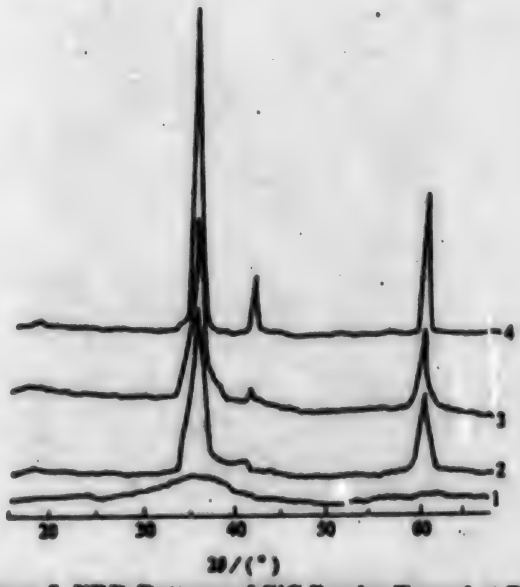

Figure 5. XRD Patterns of SiC Powder Treated at Different Temperatures

1. Not treated; 2. 1380°C; 3. 1450°C; 4. 1500°C

4. Conclusions

(1) The LPS CVD technique can produce SiC ultrafine powder. The technique is feasible because of its low processing temperature, lack of corrosion, and simple procedures.

(2) The carbon and hydrogen contents are mainly controlled by the reaction temperatures: the higher the reaction temperature, the higher the carbon content, and the lower the hydrogen content. The SiC ultrafine-powder size is controlled by the carrying-gas flow rate: the higher the flow rate, the smaller the particle size.

(3) After the transformation from LPS, the SiC powder product is always carbon rich. After the decarbonization, deoxidization, and crystallization treatment, high-purity, uniform-sized and almost completely crystallized spherical β-SiC ultrafine powder can be obtained.

References

1. Johnson, D. R., "Ceramic Technology for Advanced Heat Engines Project," DOE DE88008945, Washington, DC: DOE, 1988.

2. Chen, L. D., Goto, T., Hirai, T., "Preparation of Silicon Carbide Powders by CVD of the $(CH_3)_2SiCl_2$-H_2 System," J. MATER. SCI., 1990; 25: 4614.

3. Chen, L. D., Goto, T., Hirai, T., "Preparation of Silicon Carbide Powders by CVD of the SiH_4-CH_4-H_2 System," J. MATER. SCI., 1989; 24: 3824.

4. Cannon, W. R., Danforth, S. C., Flint, J. H., et al., "Sinterable Ceramic Powders From Laser-Driven Reaction," J. AM. CERAM. SOC., 1982; 65: 324.

5. Tanaka, H., Kurachi, Y., "Synthesis of β-SiC Powder From Organic Precursor and Its Sinterability," CERAM. INT., 1984; 14: 109.

STM Research on Nanoscale Si Thin Films

94FE0226B Beijing KEXUE TONGBAO [CHINESE SCIENCE BULLETIN] in Chinese Vol 38 No 21, 1-15 Nov 93 pp 1953-1955

[Article by Wang Zhonghuai [3769 1813 2037], Dai Changchun [2071 7022 2504], Zhang Pingcheng [1728 1627 1004], and Bai Chunli [4101 2504 4409] of the Institute of Chemistry of the Chinese Academy of Sciences (CAS), Beijing 100080, and He Yuliang [0149 1342 0081] of the Amorphous-State Research Section, Beijing University of Aeronautics and Astronautics, Beijing 100083: "Study on STM Research on Nanoscale Si Thin Film," funded by NSFC and the CAS Major Projects Fund; MS received 19 Mar 93, revised 3 Jul 93]

[Text] Nanoscale Si thin film (nc-Si:H) is a nanoscale material composed of nanoscale ultrafine crystals.[1,2] The material contains 50 volume percent of crystals, and the other 50 percent contains a large number of interface atoms which greatly affect the structure and the property of the nanoscale material.[3] Because of the novelty of the nanoscale Si thin-film structures, the film has a series of special characteristics that are different from crystalline or amorphous materials made of similar substances. These optical characteristics present application potential.[4,5]

The scanning tunneling microscope (STM) developed in the early 1980s has been widely used in different fields.[6,7] The study of polycrystalline Si thin film with STM has achieved some results,[8-11] mainly in the exploration of the film's surface characteristics and topography. However, so far there has been no report of STM research on the nanoscale material's crystal interface, which has an important effect on the structure and properties of the nanoscale material. In this paper, we utilize a locally made STM to study the surfaces of nanoscale Si thin films whose thickness varies from sub-micron to atomic scale. A series of data, especially on the crystal interface structures, is obtained.

1. Experimental Method

The nanoscale Si thin-film specimen is prepared with a plasma capacitively coupled chemical vapor deposition (PECVD) system, with highly hydrogen-diluted silane as the reaction gas, and by the excitation of an r.f. + DC double-power source.[1,2]

The instrument used in the research is a type CSTM-9000 STM for atmospheric use,[12] manufactured by the CAS Institute of Chemistry and equipped with a needle made of 80Pt-20Ir alloy (diameter: 0.25mm) by mechanical cutting or a tungsten needle (diameter: 0.25mm) made by chemical etching. In a constant-current operating mode, each image is sampled with 180 x 180 points. The surface heights are reflected by the varying shades of grayish color in the image. The voltage between the needle and the specimen tunnel junction is between 0.5 V and 2 V, with needle as positive. The maximum tunnel current selected for use has reached 1 nA, and generally is about 0.5 nA. In the following test results, the STM images are only the outcomes after the original data were smoothed. The scanning time for each image varies: from 3 min (for large images) to 15 s (for small images).

2. Results and Discussion

The STM images of nanoscale Si thin film of different magnifications in atmosphere are displayed from sub-micron to atomic dimensions. Figure 1 shows the obverse STM image of the nanoscale Si thin film obtained with the tungsten needle. The needle bias is 1 volt; and the current, 0.45 nA. The scanning areas of Figures 1(a) and 1(b) are 40.9 nm (x-direction) x 48.8 nm (y-direction), and 20.5 nm x 24.4 nm, respectively. Figure 1 shows that the nanoscale Si thin film is composed of many ultrafine particles. The densities of the surface particle arrangements vary. The particle boundaries are very clear. From Figures 1(a), and 1(b) especially, the sizes of the nanoscale Si thin-film particles can be estimated as 3 nm-5 nm, which closely coincide with the results from high-resolution electron microscopy (HREM).[1,2] The image obtained with the mechanically cut Pt/Ir needle shows comparatively smooth regions between the nanoscale particles in the nanoscale Si thin film, due to the large radius of curvature of the mechanically cut Pt/Ir needle tip.[13] Figure 2 shows the three-dimensional STM near-atomic image of the nanoscale Si thin film obtained with the Pt/Ir needle. The STM parameters are: needle bias V_t = 1.0 V; tunnel currents I_t are 0.4 nA and 0.6 nA for Figures 2(a) and 2(b), respectively; and the scanning areas are 4.10 nm x 4.88 nm and 1.7 nm x 1.0 nm, respectively. Figure 2(a) shows that the atoms in the brighter areas arrange in an orderly pattern, and the darker areas are the boundary surfaces of the crystals where the atom arrangements are somewhat random. This observation essentially coincides with Gleiter's

nanoscale material structural model.[3] Two scratch marks caused by the unstable needle are displayed in Figure 2(a). Figure 2(b) displays the orderly arrangement of atoms with a distance of about 3 Angstroms between neighboring atoms. At this position, we believe that the area of STM observation is focused on the particle. Since the particle is crystalline,[1,2] the orderly arrangement of the atoms is observable.

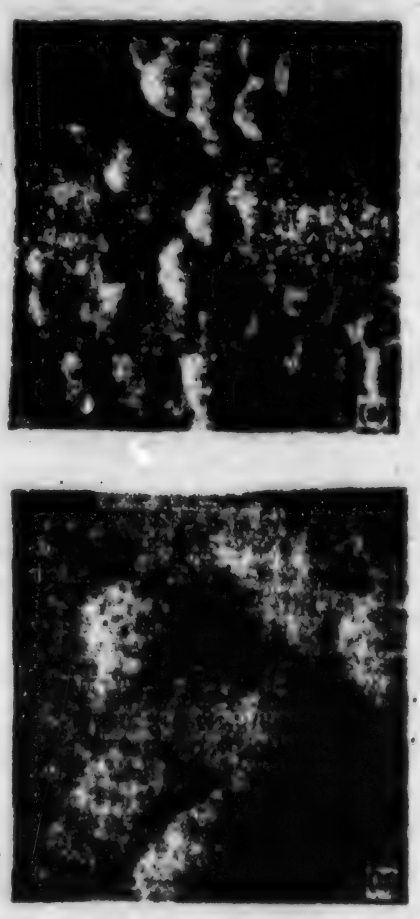

Figure 1. Plane Image of Nanoscale Si Thin Film

Scanning area: (a) 40.9 nm x 48.8 nm, (b) 20.5 nm x 24.4 nm

This experiment has found that the needle bias for image formation should not be too low to cause needle instability, which is probably due to the nanoscale Si thin-film surface oxidation. On the other hand, during the preparation of the nanoscale Si thin-film specimen, the reaction between silicon and hydrogen may hinder the surface oxidation. These results are only preliminary. Further study is in progress.

3. Conclusions

The STM study of nanoscale Si thin film reveals that this film is composed of nanoscale particles with

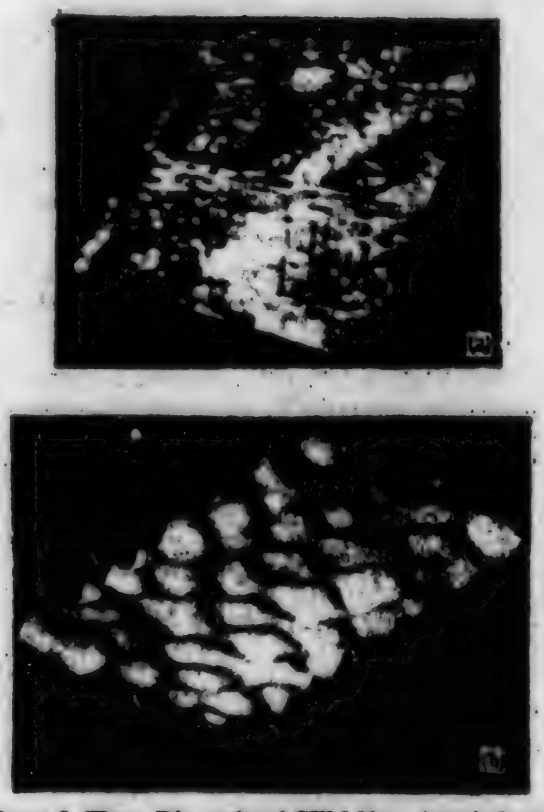

Figure 2. Three-Dimensional STM Near-Atomic Image of Nanoscale Si Thin Film

Scanning area: (a) 4.10 nm x 4.88 nm, (b) 1.7 nm x 1.0 nm

average particle size of 3 nm-5 nm. Through the STM's high-resolution imaging capability, the near-atomic images on the thin-film surface are directly observed. The images show that the atom arrangement of the nanoscale particles is orderly, and the atom arrangement between the particles is comparatively random. These results coincide with past observations by HREM, and further disclose the microstructure of the nanoscale Si thin film.

Acknowledgment: The authors are grateful to Research Fellow Xu Yiming and Senior Engineer He Liang of the CAS Institute of Semiconductors and to Professor Lin Hongyi of Beijing Institute of Technology for their enlightening discussions.

References

1. He Yuliang, Yin Chenzhong, Cheng Guangxu, et al., BANDAOTI XUEBAO [CHINESE JOURNAL OF SEMICONDUCTORS], 1992, 13(11): 683-689 [English abstract in JPRS-CST-93-001, 7 Jan 93 p 35].

2. He Yuliang, Liu Xiangna, Wang Zhichao, et al., ZHONGGUO KEXUE, Series A, 1992, (9): 995-1001 [abstracted in JPRS-CST-93-001, 7 Jan 93 p 7].

3. Gleiter, H., EUROPHYSICS NEWS, 1989, 20(9): 130-133.

4. Zook, J. D., APPL. PHYS. LETT., 1980, 37(2): 223-226.

5. Ashburn, P., Soerowirdjo, B., IEEE TRANS. ELECTRON DEVICES, 1984, Ed-31, 853-860.

6. Bai Chunli, ed., "Scanning Tunneling Microscopy and Its Applications," Shanghai Science and Technology Press, 1992 [in Chinese].

7. Wang Zhonghuai, Dai Changchun, Sun Hong, et al., KEXUE TONGBAO [CHINESE SCIENCE BULLETIN], 1993, 38(5): 433-435 [translated in full in JPRS-CST-93-013, 27 Jul 93 pp 10-11].

8. Gimzewski, J. K., Humbert, A., Pohl, D. W., SURFACE SCIENCE, 1986, 168: 795-800.

9. Hosaka, S., Sagara, K., Hasegawa, T., et al., J. VAC. SCI. TECHNOL., 1990, A8(1): 270-274.

10. Carrejo, J. P., Thundat, T., Nagahara, L. A., et al., J. VAC. SCI. TECHNOL., 1991, E9(2): 955-959.

11. Sugawara, Y., Fukano, Y., Kamihara, Y., et al., ULTRAMICROSCOPY, 1992, 42-44: 1372-1375.

12. ixBai Chunli, KEXUE TONGBAO [CHINESE SCIENCE BULLETIN], 1989, 34(5): 339-340.

13. Musselman, I. H., Russell, P. E., J. VAC. SCI. TECHNOL., 1990, A8(4): 3558-3562.

Raman Spectroscopy of Nanoscale SnO_2

94FE0226C Beijing KEXUE TONGBAO [CHINESE SCIENCE BULLETIN] in Chinese Vol 38 No 21, 1-15 Nov 93 pp 2014-2015

[Article by Zuo Jian [1563 1696], Xu Cunyi [6079 1317 5030], Liu Xianming [0491 0341 2494], and Wang Changsui [3769 2490 3606] of the Structural Analysis Open Laboratory, and Wang Chengyun [3769 2052 0061], Hu Yuan [5170 3293], and Qian Yitai [6929 6654 3141] of the Department of Applied Chemistry, University of Science and Technology of China (USTC), Hefei, 230026: "Study of Raman Spectroscopy of Nanoscale SnO_2," funded by NSFC and the USTC Structural Analysis Open Laboratory Foundation]

[Text] SnO_2 nanoscale crystal powder is prepared with a hot-water method as follows: The metallic tin powder is mixed with nitric acid and the reaction turns the mixture into a transparent solution. The solution is then mixed with polytetrafluoroethylene and loaded in an autoclave at 150°C for 24 hours. After the treated solution is cooled to room temperature, white SnO_2 powder is obtained. The powder is washed thoroughly, baked at 150°C for 24 hours, and then pressed into a plate under a pressure of 10^5 kg/cm^2. The initial particle size of the specimen is 3 nm. After annealing at different temperatures, nanoscale SnO_2 powders of different particle sizes are obtained. The powder crystal structure belongs to the rutile type, and there is less than 1 percent of impurities in the powder.

The Raman spectrum is measured with a U.S. SPEX-1403 laser Raman spectrometer. The excitation light is the 514.5-nm line from an argon-ion laser. The back-scatter configuration is adopted. All measurements are conducted at room temperature.

Figure 1 shows that the peaks in the Raman spectra are of two different groups: the peaks in one group, called mode A, correspond with the peaks in the monocrystalline or polycrystalline SnO_2 spectra. The Raman spectrum peaks with wave numbers of 472, 632, and 773 cm^{-1} are designated as A_1, A_2, and A_3, respectively. In the other group, called mode B, the peaks with wave numbers of 358 and 572 cm^{-1} are designated as B_1 and B_2, respectively. The mode-B peaks do not exist in the monocrystalline or polycrystalline SnO_2 Raman spectra. This observation indicates that the appearance of B_1 and B_2 peaks is caused by the nanoscale effect.

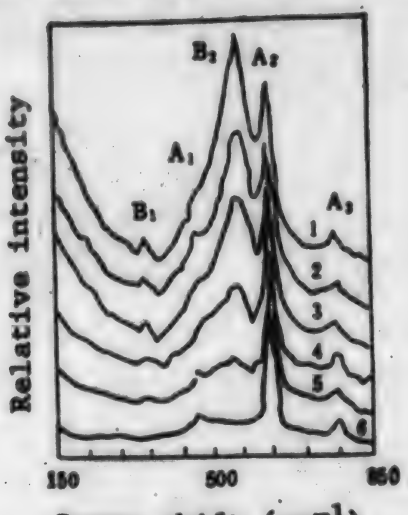

Figure 1. Raman Spectra of Different Nanoscale SnO_2 Solids

1-6 are 3, 4.4, 6.5, 9, 13, and 90 nm, respectively

All the peak intensities in Figure 1 are normalized according to the intensity of peak A_2. As shown in Figure 1, the intensity ratios of the peaks in mode B to the peaks in mode A increase rapidly with decrease in

crystal size. This observation is similar to the phenomenon wherein surface-atom fractions rapidly increase with decrease in crystal size. We assume that the B_1 and B_2 peaks are caused by the surface phonon modes and are closely related to the A_1 and A_2 peaks. This experiment shows that the frequencies of the B_1 and B_2 peaks are lower than those of the A_1 and A_2 peaks. The appearance of the low-frequency surface phonon modes is induced by the relaxation among the surface atoms. This relaxation weakens the interaction among the surface atoms, and consequently reduces the surface force coefficient.

Calculations based on the Raman spectra of nanoscale solid materials are expected to generate the specific positions of the nanoscale surface atoms.

Acknowledgment: The authors are grateful to Professors Qian Linzhao and Zhu Qingshi for their interest and guidance throughout this research.

Design, Preparation of MgO/Ni Functionally Gradient Materials

94FE0227A Beijing GUISUANYAN XUEBAO [JOURNAL OF THE CHINESE CERAMICS SOCIETY] in Chinese Vol 21 No 5, Oct 93 pp 406-412

[Article by Zhang Lianmeng [1728 5144 4145], correspondent, Tang Xinfeng [0781 2450 1496], Chen Fuyi [7115 4395 5030], and Zhang Qingjie [1728 3237 3638] of the State Key Laboratory for Synthesis and Processing of Advanced Materials, Wuhan University of Technology: "Design and Preparation of MgO/Ni Functionally Gradient Materials"; MS received 9 Jun 92]

[Text]

Abstract

The property parameters for thermal-stress optimization design of the MgO/Ni-system functionally gradient materials (MgO/Ni FGM) are determined by experimental measurements as well as by calculations according to a micromechanical model. The causes of different results achieved by these two methods are discussed. The finite element method is used to simulate the thermal stress in FGM during its preparation. The consolidated rules for MgO/Ni FGM design postulation are obtained. Based on design results, progressive adjustments of powder technology properties are made. Consequently, MgO/Ni FGM is successfully sintered.

Key words: Functionally gradient material, thermal stress, microstructure, design, preparation.

1. Introduction

Metal/ceramic-system functionally gradient materials (FGMs) are new composite materials having applications potential in such high-tech fields as aerospace, nuclear energy, etc.[1] Whether they can eventually be put into practical application depends on the crucial elimination of fractures caused by the thermal stress induced from different gradient layer properties.

MgO/Ni-system sintered bodies of various compositions are prepared by the powder spreading-filling method. Their basic property parameters for thermal-stress optimization design are measured. The causes of differences between these parameters and calculated values are discussed. Based on test data, the thermal stress induced during the MgO/Ni-system FGM (MgO/Ni FGM) preparation is simulated with the finite element method, and based on the consolidated analysis of the magnitudes and distributions of stresses, a principle of material structure and composition distribution is proposed. Guided by design results and considerations of such production technology factors as strengths of the transition layers and property data, as well as sintering shrinkage and densification conditions, MgO/Ni FGM plates are prepared.

2. Measurement and Evaluation of Property Parameters

2.1 Material System Selection and Preparation for Sintered Bodies of Different Compositions

The MgO/Ni composite system is selected because of MgO ceramic's superior high-temperature stability, high-temperature basic vapor corrosion resistance, high-temperature insulation, etc. Additionally, the thermal expansion difference between MgO and nickel is small. The gradient combination of these two materials has high potential to be used as the inner-wall material for the ducts of magnetohydrodynamic generators.[2]

The raw materials are MgO microfine powder and nickel carbonyl powder. Both materials have greater than 99.5 percent purity. The particle size for MgO is 0.3 μm; for nickel carbonyl powder, 5 μm. Each of the powder mixes of different MgO/Ni volume compositions is loaded in a separate pack and isostatically compacted under 100 MPa pressure. The pressed specimens are then sintered in 1.0×10^{-2} Pa vacuum. Considering the nickel sintering temperature, we set the sintering conditions at 1300°C for 100 minutes. The sintered bodies are cut and polished for experimentation.

2.2 Properties of Sintered Specimens

The specimen property parameters of six sintered compositions are measured. Their results are listed in the following table.

Material Properties for Various MgO/Ni Mixture Volume Ratios

Specimen No.	A	B	C	D	E	F
Volume fraction of MgO φ/%	100	80	60	40	20	0
Relative density d_r/%	71	64	62	72	83	93
Young's modulus E/GPa	104	52	60	56	105	146
Bending strength σ_b/MPa	74	49	29	42	108	163
Poisson's ratio ν	0.16	0.18	0.27	0.26	0.26	0.35
Thermal expansion coefficient α x $10^6/K^{-1}$	12.8	12.9	13.5	14.3	14.5	15.1

The table shows that the bending strengths of the sintered specimens are closely related to their relative densities. The lowest relative density of specimen C corresponds to its lowest bending strength. In addition, among the three major property parameters for finite element simulation, only the thermal expansion coefficient α has an approximately linear relationship with the volume fraction; the other two values, Young's modulus E and Poisson's ratio ν, obviously depend on the microstructure of the sintered specimens. Figure 1 shows the variation of the measured data of relative density and Young's modulus with the volume fraction of nickel. Figure 2 shows the variation of thermal expansion coefficient and Poisson's ratio with the volume fraction of nickel. For analytical convenience, the figures also contain the curves denoting the corresponding property changes with the changing of composition calculated from the micromechanical model of Wakashima.[3] When the nickel content is increased, the variation patterns of the calculated values and the experimental values of the sintered specimen's Young's modulus are similar, except at the point of 40-volume-percent nickel; besides, the calculated density variations correspond to the experimental variations. The calculated value of E is minimum at 60 volume percent of nickel; however, the fact that the experimental E is not minimum at 40 volume percent of nickel but higher than the E values of the two neighboring points indicates that Young's modulus is strengthened at this point. The strengthening characteristic also occurs in Poisson's ratio ν. At the same point of 40-volume-percent nickel fraction, the value of ν is 0.27, which is also higher than the ν values of the two neighboring points. The phenomenon that material property parameter at a certain composition displays abnormal strengthening, which disagrees with the Wakashima equation, is caused by the exceptional sintered microstructure at that particular composition. Experiments show that specimens B, D, and E display typical dispersion structures, i.e., MgO as second phase disperses in the nickel matrix, or vice versa. However, the microstructure of specimen C is different, as it displays a geometric network structure with a continuous crisscross of nickel and MgO. This network structure strengthens E and ν. Since Wakashima's model is based on the sparse-dispersion micro-geometrical structure, it cannot describe the properties of materials with network structures.

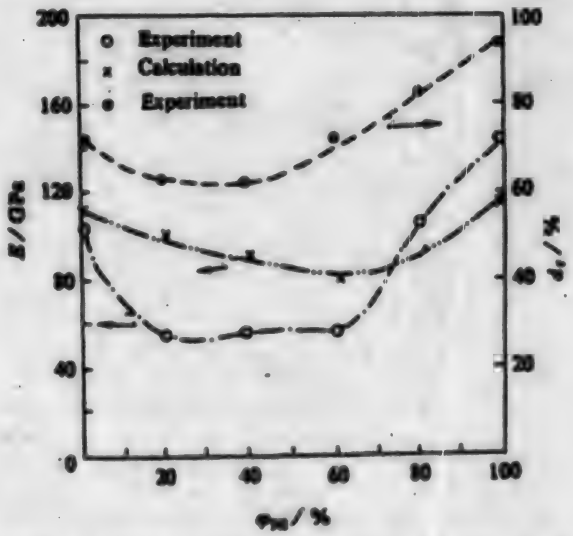

Figure 1. Young's Modulus and Relative Density vs. the Volume Fraction of Ni

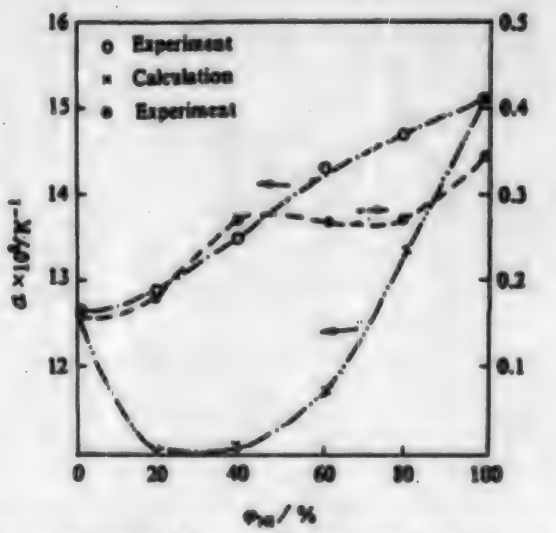

Figure 2. Thermal Expansion Coefficient and Poisson's Ratio vs. the Volume Fraction of Ni

3. Thermal Stress Simulation and Structural Design

3.1 Computed Model

The computed model uses the prepared disk specimen, 6mm thick and 30mm in diameter, which is sliced into 15 layers according to the composition. The specimen is cooled to room temperature from 1000°C. The measured properties are used as model parameters. The properties of the intermediate gradient layers are obtained through interpolations of the tested data. A power function is used to describe the volume fraction variations of different gradient layers. The composition distribution curves from different indices P are expressed by the equation $C = (x/d)^P$;[4] where d is the total thickness of each gradient layer, x is the position coordinate of any gradient layer, and P is the distribution index which determines the configuration of the composition distribution curve C. At the plate's ¼ cross section, we make the finite-element network partitions, and assign different composition distribution indices accordingly, then simulate the thermal stress in the specimen with the finite element method.

3.2 Analysis of Computed Results

In the computation, the P value varies from 0.6 to 2.8. The results show that a distinct thermal relaxation effect occurs for any FGM composition distribution, and the maximum stress boundary moves toward the nickel-rich side. When P = 0.6, the maximum radial stress component σ_{rr} is 96 MPa, which indicates a thermal stress relaxation rate of 35 percent, as compared with the thermal stress of the double-layered Ni-MgO FGM (NFGM); when P = 1.8, the relaxation rate is as high as 70 percent.

Figure 3 shows the variation of the maximum σ_{zz}, σ_{rr}, and $\sigma_{\theta\theta}$ with the P values. All three stresses have minimum values in the areas of P variations and all appear in the neighborhood of P = 1.8. Comparatively speaking, the axial stress σ_{zz} is very small, about ¼ of the radial stress σ_{rr} and the ring stress $\sigma_{\theta\theta}$. This is due to the fact that for the FGM specimens of this experiment, the ratio of the gradient thickness to the diameter is 0.13. Large axial stress cannot be induced from this small thickness-to-diameter ratio.[4] Therefore, the FGM structural design must take σ_{rr} and $\sigma_{\theta\theta}$ as the main control stresses.

Figure 3 shows that the σ value is minimum when P = 1.6 to 1.8. Whether this P value would provide the best design will be discussed later in this paper. Figure 4 shows the variation of maximum stress location center with index P (in the graph, h is the distance from the center line to the pure nickel side). Figure 4 also shows

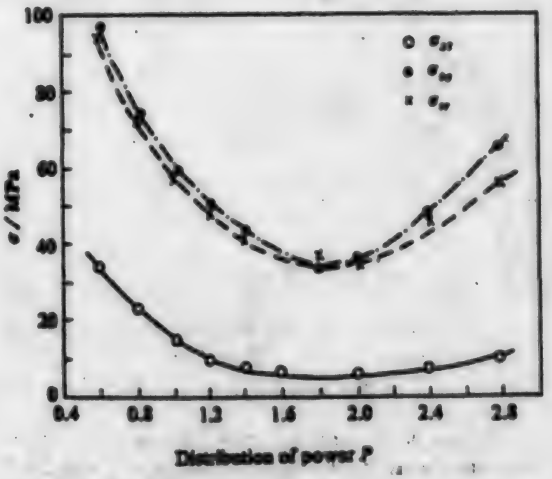

Figure 3. Maximum Thermal Stresses vs. Various Compositional Distribution Power

the corresponding FGM gradient layer to the maximum stress location. We can see that the location of the maximum stress changes with the P value. After the P value reaches 1.2, the location of the maximum stress center drops sharply; as the P value continuously increases the maximum stress center moves downward and approaches the model's symmetrical center line. The right coordinate of Figure 4 shows that the center line is located at the layer with 40 percent of MgO, which is the weaker section (measured value is 42 MPa) of the gradient material. Comparing with Figure 3, we can see that even when P = 1.8, the stress is at the minimum value of 40 MPa; this minimum value is very close to the allowable material strength; hence, the failure would naturally occur at the center line of the radial direction. When P = 1.0, the maximum stress center occurs at 0.8 h, which is the straight nickel layer. Referring to both Figure 3 and Figure 4, although σ_{rr} and $\sigma_{\theta\theta}$ are comparatively high (about 60 MPa), they are still far below the actual test strength (163 MPa) of the straight nickel layer. Besides, t[illegible] computed stress diagram also shows that when the P value changes, even though the straight ceramic side is generally under compressive stress, a tensile symptom still displays at the neighborhood of the circumference of 0.9 R (R is the radius of the round FGM plate) on the horizontal surface and the axial direction of the ceramic side. The tensile stress, however small (especially σ_{zz}), should be included in the analysis. As shown in Figure 5, the local tensile stress on the straight ceramic side at P = 1.6 is minimum. When P = 1.8, the local tensile stress σ_{rr} and $\sigma_{\theta\theta}$ are both smaller than 40 MPa, which is far smaller than the allowable measured strength.

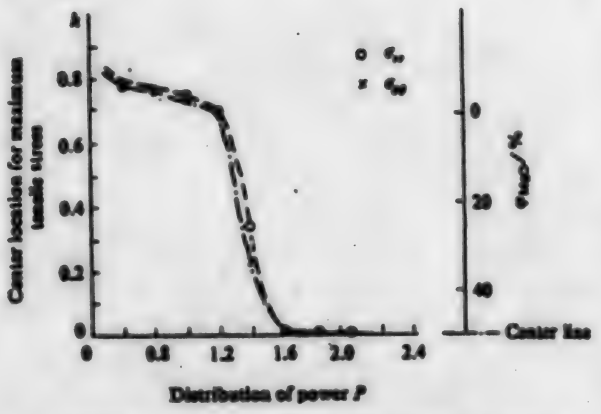

Figure 4. Maximum Stress Location vs. Various Compositional Distribution Power; h is a half thickness of the sample

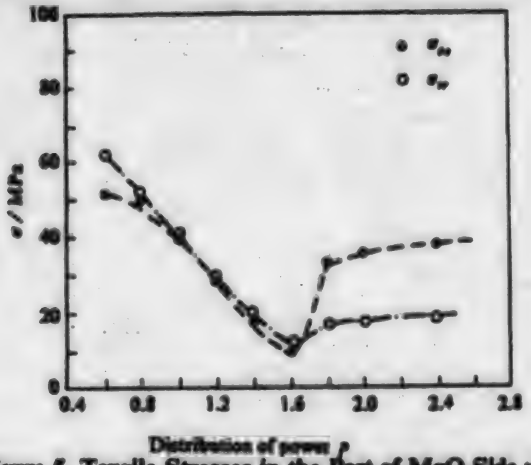

Figure 5. Tensile Stresses in the Part of MgO-Side vs. Various Distribution Power

In conclusion, even the composition distribution index P that represents the best thermal stress relaxation effect cannot completely reflect the correct structural control parameters. All the following three conditions must be considered:

(1) the target P value which represents the minimum thermal stress;

(2) the adjusted P value so that the location of thermal stress occurs as close to the metallic side as possible;

(3) whether the corresponding P value would induce a tensile stress far smaller than the allowable strength on the straight ceramic side.

Based on these considerations, the best FGM design can be obtained and the FGM material composition distribution can be determined. This is the basic principle of structural design to avoid fractures in the FGM during its preparation. Based on the above, the design outcome is P = 1.0.

4. Preparation of Functionally Gradient Materials

MgO/Ni FGMs are prepared according to the design result P = 1.0. Fifteen layers of MgO/Ni powder of different compositions are piled by the layer-filling technique, then the green compacts are either vacuum sintered, or hot-pressing (HP) sintered.

4.1 Adjustment of Compacting and Sintering of Powder Mix

During vacuum FGM sintering, in the periods of temperature rising, sintering, and cooling, the compacts are not constrained by any external forces. Therefore, adjustments of the compacting property and the sintering property are possible, which is particularly important for a defect-free specimen. In this experiment, two different types of MgO powder, both mixed with 0.5 weight percent of Fe_2O_3 powder, are used. One is fluffy microfine powder decomposed from $Mg(OH)_2$. The average particle size is about 0.3 μm. The other is fine powder thermally decomposed from $MgSO_4$-$7H_2O$. The average particle size is about 3 μm. When the mixes are made of exclusively 0.3 μm fluffy powder and nickel powder, the variation of compacting densities and sintering shrinkages with the MgO composition is as shown in Figure 6. Because of the considerable variations among the specimen compact densities (especially in the straight ceramic specimens, the differences between the axial pressed compacts and the compacts further treated with 100 MPa cold isostatic pressing are very wide), and the relatively low final straight ceramic compact density, stress-induced cracks frequently occur on the straight ceramic side of the laminated compacts. To solve this problem, 15 to 35 weight percent of large-particle (d = 3 μm) MgO powder is added. The addition of large-particle MgO powder increases the MgO compact density, and also reduces the shrinkage differences among the sintered specimens. The previous table shows that the densification rates of all specimens used in structural designs are fairly low with high degrees of porosity, which is mainly affected by the sintering parameters and densification technique. To meet the sintering temperature of nickel powder and reduce the densification sintering temperature of MgO so that the sintering properties of nickel powder and MgO become compatible, about 0.5 weight percent of Fe_2O_3 powder is added.[3] After this treatment, almost all the specimen relative densities reach 90 percent after sintering at 1320°C for 2.5 hours.

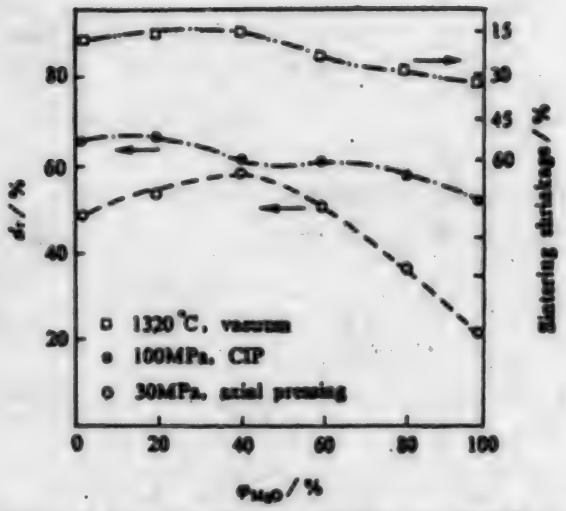

Figure 6. Formation Density and Sintering Shrinkage for MgO/Ni Mixtures

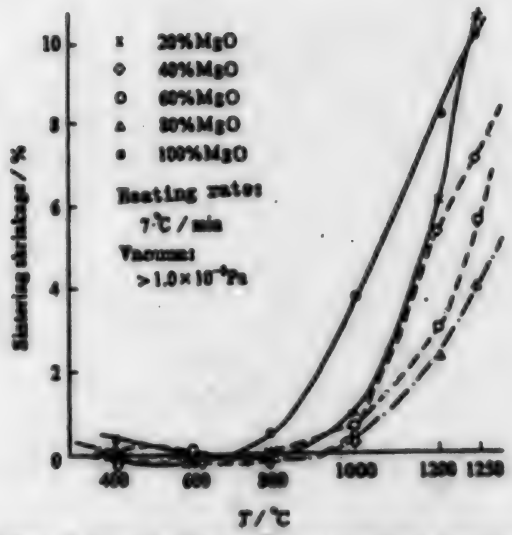

Figure 7. Sintering Shrinkage of MgO/Ni Mixtures With Various Mixing Ratios

After the aforementioned adjustments, the green compacts of various compositions are used to determine the sintering shrinkage rate changes from room temperature up to 1250°C at a constant temperature increasing rate. The results are shown in Figure 7. For all but the straight MgO specimen, the sintering shrinking rate increases with the increase of nickel content, but the difference of the shrinkage magnitudes between any two neighboring specimens is small. Basically, a balance of the sintering shrinkages is achieved. The straight MgO specimen contains about 70 weight percent of microfine powder, and produces an uncoordinated shrinking situation with its neighboring layers. During the FGM's actual lamination, compaction, and sintering, the straight nickel side has a higher compaction density due to irostatic cold pressing. Hence the diameter of the ceramic side is larger than that of the straight metal side (by about 6 percent). However, the "uncoordinated" shrinkage offsets the existing dimension difference during compaction, and eventually a uniform FGM specimen is prepared.

In conclusion, quality FGM can only be made according to the basic structural design principles when the preparation conditions such as powder particle size, additives, compact deformation, sintering shrinkage, etc. are adjusted and controlled in coordinated fashion.

4.2 Preparation of FGM

Two FGM disc specimens of the MgO/Ni system with about 6mm thickness, and diameters of 24mm and 30mm are made by vacuum sintering and HP sintering, respectively. The vacuum sintering parameters are as follows: 1320°C, 2.5 hours, and 1 x 10^{-2} Pa vacuum; and the HP sintering parameters: 1300°C, 28 MPa pressing pressure, and 1 hour. Figure 8 shows the prepared specimens. During the HP sintering, the pressure is released at about 1000°C, and MgO displays high-temperature plastic deformation,[6] hence, the thermal stress is sufficiently relaxed in the course of HP sintering to pressure releasing. Therefore, the specimen prepared by HP sintering has a larger diameter and no surface defects.

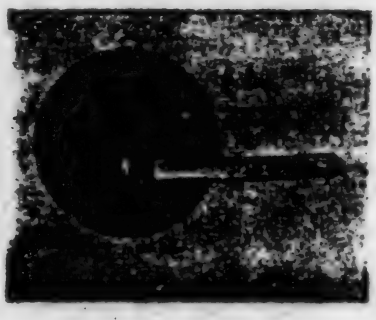

(a) HP sintering

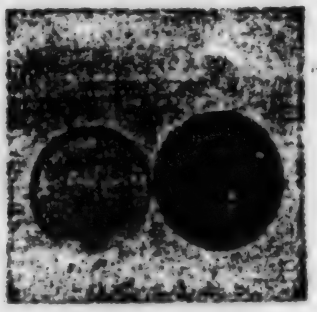

(b) Vacuum sintering

Figure 8. MgO/Ni FGM Samples Prepared by Different Sintering Methods

5. Conclusions

(1) The experimental method and the micromechanical model are used to measure and calculate the property parameters of the sintered bodies of the MgO/Ni system with various compositions. The results show that the specimen's sintering strength is mainly controlled by porosity; the coefficient of thermal expansion follows a quasi-linear variation; and Young's modulus and Poisson's ratio are strengthened at 40 volume percent of nickel content. The implication is that Wakashima's micromechanical model cannot yet truthfully describe the micro-network structure of the sintered body.

(2) The thermal stress simulation of a FGM model with a thickness-to-diameter ratio of 0.13 shows that compared with NFGM, FGM clearly has a thermal stress relaxation effect, and the maximum stress boundary layer moves significantly toward the metal side. The degree of relaxation depends on the distribution index P. The minimum values of the three major stress components occur when P = 1.8 (when the stress relaxation is 70 percent).

(3) However, the best material structural design condition is not when P = 1.8. When factors such as the structural location of the maximum stress, the strength of the gradient layer at the same location of the maximum stress, and furthermore, the tensile strength of the straight ceramic side are considered, the best combined design condition for MgO/Ni FGM is when P = 1.0.

(4 Based on P = 1.0, when factors such as raw-material particle size, sintering properties, and the balance between compact contraction and sintering shrinkage are adjusted, FGM of the MgO/Ni system without macroscopical surface defect can be prepared by vacuum sintering and HP sintering methods.

References

1. Niino, Masayuki; Hirai, Toshio; Watanabe, Tatsuzo, "Functionally Gradient Materials—Toward Applications of Ultra-Heat-Resistant Materials in Space Mechanics" [in Japanese] JOURNAL OF THE JAPAN SOCIETY FOR COMPOSITE MATERIALS, 1987; 13: 257.

2. Nishida, Toshihiko, and Shiono, Takeshi, "Fabrication of Magnesia Stainless Functionally Gradient Materials via Hot-Press Process" [in Japanese], MATERIALS, 1990; 39: 438.

3. Wakashima, K., Tsukamoto, H., "Micromechanical Approach to the Thermomechanics of Ceramic-Metal Gradient Materials," in: Yamanouchi, M., et al., eds., Proc. of the 1st Int. Symp. on FGM (Sendai), 1990: 19.

4. Kawasaki, A., Watanabe, H., "Microstructure Designing and Fabrication of Disk-Shaped Functionally Gradient Material by Powder Metallurgy," J. JPN. SOC. POWDER METALL., 1990; 37 (2): 76.

5. Hamano, K., Fukuhara, T., "Effects of Addition of Fe_2O_3 on Microstructure of Magnesia Ceramics," in: Hirano, S., ed., 26th Symp. of Basic Sci. of Ceram., Jpn., 1988, (Nagoya) Japan.

6. Kingery, W. D., Bowen, H. K., Uhlmann, D. R. "Taoci Daolun" [Introduction to Ceramics] (translated by Qinghua University), Beijing, China Building Industry Press, 1982: 715.

Microcomputer C-Ada Compiling System Certified

94P60123A Beijing GUANGMING RIBAO in Chinese 11 Jan 94 p 2

[Article by Meng Fansen [1322 4907 2773] and Li Dan [2621 0030]: "Nation's Computer Compiling Technique Strides into Advanced Ranks"]

[Summary] The high-level microcomputer C-Ada compiling system perfected by a Beijing Sanjiu [0005 0046] Enterprises Corporation research team led by Professor Li Xin [2621 6580] recently passed the formal appraisal conducted by a panel of 15 software experts. An especially interesting feature of this system is the originality of its parallel processing capabilities, in which—it is reported—China ranks second in the world.

Nation's Computer Industry Records First Trade Surplus

94P60105A Beijing JISUANJI SHIJIE [CHINA COMPUTERWORLD] in Chinese No 50, 29 Dec 93 p 1

[Article by Liu Keli [0491 0344 7787]: "Nation's Computer Industry Enters Benign Cycle: Import and Export Trade Turnover Has First Surplus"]

[Summary] China's computer industry import and export trade turnover this year recorded its first surplus. According to official statistics, the nation's 1993 gross volume of computer imports and exports was US$2.139 billion, of which imports amounted to $1.05 billion and exports to $1.088 billion. This first trade surplus for the 30-odd-year-old domestic computer industry indicates that this industry has entered the development phase of a benign cycle [between economic activities].

While exports of computer hardware parts and boards continue to form the bulk of China's computer exports, a growing percentage comes from application software and other kinds of software. Analyzing the reasons for the nation's first computer-industry trade surplus, Yang Tianxing [2799 1131 5887], director of the Ministry of Electronics Industry's Computer Department, commented that the dominant position of China's computer industry in terms of labor, talent, and technology is gradually coming into play amid international market competition, and that the production scale of the three types of foreign-funded enterprises is gradually growing—both reasons being critical factors for foreign-exchange-earning exports.

China, U.S. Jointly Develop FDDI Cards for Information Highways

94P60105B Beijing KEJI RIBAO [SCIENCE AND TECHNOLOGY DAILY] in Chinese 5 Jan 94 p 2

[Article by Cao Bo [2580 3134]: "China, U.S. Jointly Develop Optical Fiber Interface Cards: Often Called [the Heart of] Computer 'Highways'"]

[Summary] Fiber Distributed Data Interface (FDDI) cards, often called the heart of computer data "highways," have been jointly developed by Chinese and U.S. scientists. Saishite [6357 0013 3676] Electronics Ltd. of Shenzhen has pioneered domestic batch production of the cards, and authoritative sources say that this demonstrates China is now in the world's front ranks in the field of computer high-speed [100 Mbits/s] local area networks, or LANs.

In the past, China has had to expend large amounts of foreign exchange for imports of fiber optic network cards. But in September 1993, the Shenzhen firm put out its first card, filling a domestic void. Now, the FDDI cards have been authenticated by the U.S. Federal Communications Commission, and have rapidly entered the domestic and foreign markets.

IBM Buys Patent Usage Rights for Wangma's Character-Input Technique

94P60120A Beijing RENMIN RIBAO OVERSEAS EDITION in Chinese 2 Feb 94 p 2

[Unattributed article: "U.S. IBM Corp. Buys 'Five-Stroke Character Type' Patent Usage Rights"]

[Summary] Beijing (XINHUA)—The U.S. firm IBM Corporation recently in Beijing reached formal agreement with Beijing Wangma [3769 4316] Computer Corporation to purchase rights to use the patented "Five-Stroke Character Type" [wu bi zixing] computer Chinese-character input technique. This technique, invented by Wangma Computer Corp. Governor Professor Wang Yongming [3769 3057 2494], has been patented in three nations—the U.S., Britain, and China. The technique covers 90 percent of domestic computer users and has found applications in the U.N. and Southeast Asia. The U.S. firm DEC and the Japanese firm Casio already reached agreement with Wangma Corp. for rights to use this patented technique, which has become for foreign computer makers a "key" to opening up the China market.

Fifth-Generation Industrial Robots on Market

94P60099A Beijing RENMIN RIBAO OVERSEAS EDITION in Chinese 10 Jan 94 p 3

[Article by Xu Jingyue [1776 0079 6460]: "Nation's Robotics Research Ascends to Advanced International Level: Fifth-Generation Industrial Robots Now on Market"]

[Summary] Beijing, 8 Jan (XINHUA)—Nine varieties of domestic fifth-generation industrial robots are now on the market. These robots—used for arc welding, spot welding, spray painting, assembly, transport, teaching, research, and handling of toxic substances and explosives—meet advanced international standards for variety, performance, quality, and reliability.

The arc-welding and spot-welding robots, developed by the China Aerospace Corporation's (CASC) Institute 17 along with other units, have "teaching and playback" intelligent functions. The spray-painting robot, developed by CASC's Institute 706 along with other units, can grasp 10-kg objects and has a repeat positioning accuracy of 2mm. An electronic-component mounting robot with visual recognition functions has a repeat positioning accuracy of 0.03mm. These robots are now in batch production, and have found applications in the arc-welding and spray-painting assembly lines for the "Audi" bus, made at the No. 1 Automotive Works, and the "Dongfeng" [East Wind] truck, made at the No. 2 Automotive Works.

[Photo caption with text by XINHUA staff writer and photography by Bai Lianguo] The nation's first 7-degrees-of-freedom robot recently passed ministry-level appraisal at Beijing University of Aeronautics and Astronautics (BUAA). The photograph shows the robot during an obstacle-avoidance demonstration. This 7-joint robot has realized "self-motive" and kinematic in-line real-time optimized control.

Sino-Canadian 'Global Radar Remote Sensing Plan' Flights Completed

94P60112A Beijing ZHONGGUO KEXUE BAO [CHINESE SCIENCE NEWS] in Chinese 3 Jan 94 p 2

[Article by Liu Quanrui [0491 5425 3843]: "Global Radar Remote Sensing Plan Successfully Implemented in Guangdong"]

[Summary] Guangzhou (ZHONGGUO KEXUE BAO report)—As part of the "Global Remote Sensing Plan" jointly developed by the CAS Institute of Remote Sensing Applications and the Canadian National Remote Sensing Center, engineers on 21 and 22 November [1993] flew over the Zhaoqing Prefecture of Guangdong Province and successfully completed radar remote sensing flight imaging tasks including real-time acquisition of perfectly clear images. These images, to be used for development and exploration of agricultural, forest, mineral, and water resources, were captured with a high-resolution side-looking synthetic aperture radar (SAR) and other advanced instruments carried on board the Canadian CV-580 aircraft flying at an altitude of 5,500 meters and having an imaging range of over 8,000 square kilometers. The current cooperative project with Canada, in addition to the aforementioned radar imaging flights, also included a symposium, data processing and analysis, and academic interchanges. Chinese scientists and engineers commented that the project will inevitably improve the nation's technological level in radar remote sensing, and scientists on both sides expressed satisfaction with the successful implementation of the plan flights.

Beijing FEL Achieves Saturated Oscillation

94P60112B Beijing RENMIN RIBAO OVERSEAS EDITION in Chinese 15 Jan 94 p 3

[Article by Yang Lianghua [2799 5328 0553]: "Beijing Free Electron Laser Facility Achieves Another Major Breakthrough: Successfully Realizes Saturated Oscillation, a State-of-the-Art Accomplishment"]

[Summary] Beijing, 14 Jan (RENMIN RIBAO OVERSEAS EDITION report)—This writer learned today from sources at the CAS Institute of High-Energy Physics that the institute's Beijing Free Electron Laser (BFEL) facility, which achieved infrared FEL oscillation over six months ago [see JPRS-CST-93-013, 27 Jul 93 p 18], recently had another major breakthrough. On 28 December 1993, the BFEL facility successfully realized saturated oscillation, becoming Asia's first infrared FEL facility—among the 10-odd such installations built in the United States, West Europe, and then Asia—to reach this goal and thus propelling China into the world's front ranks in this high-tech field. The BFEL facility first achieved infrared FEL oscillation on 26 May last year, making China the fourth nation—after the United States, the Netherlands, and France—to use a radio-frequency linear accelerator for generating infrared FEL light. Following that achievement, BFEL facility scientists succeeded in raising the electron beam density and improving the uniformity of the quality factor; this in turn permitted them to raise system gain from the original 6 percent to 17 percent, where saturated oscillation took place. Also, compared to last May's achievement, stimulated oscillation signal strength is now 5 orders of magnitude higher [i.e., 100,000 times as high] and spontaneous radiation strength is 8 orders of magnitude higher.

Method of Focusing Control for VISSR of GMS in Orbit

94P60098A Shanghai HONGWAI YU HAOMIBO XUEBAO [JOURNAL OF INFRARED AND MILLIMETER WAVES] in Chinese Vol 12 No 4, Aug 93 pp 261-264

[Article by Zhu Guangze [2612 1639 6358] and Wei Caiying [7614 1752 5391] of the National Satellite Meteorology Center, SMA, Beijing 100081: "Method of In-Orbit Focusing Control for VISSR of Geostationary Meteorological Satellite" (GMS); MS received 4 Jun 92, revised 25 Apr 93]

[Abstract] Based on the theory of MTF (modulation transfer function) in Fourier optics, the features of a VISSR (visible-infrared spin scan radiometer) optical imaging system are analyzed. A criterion and method for VISSR focusing are proposed and the experimental results for frequency-spectrum analysis using fast Fourier transforms (FFT) on stretched digital cloud images received from the Japanese GMS-4 satellite are given. The tests show that this method is useful and practical for in-orbit focusing control of a GMS's VISSR.

Figure 1, not reproduced, is a flow chart for VISSR focusing. Figure 2, reproduced below, depicts the system equipment. There are no tables.

References

1. Zhang Youwen, "Infrared Optical Engineering" [in Chinese], Shanghai: Shanghai Science and Technology Publ. House, 1982, pp 293-396.
2. Mai Weilin, "Optical Transfer Functions and Their Mathematical Foundations" [in Chinese], Beijing: National Defense Industry Publ. House, 1979, pp 1-47.
3. Sun Zhongkang, Shen Zhenkang, "Digital Image Processing and Its Applications" [in Chinese], Beijing: National Defense Industry Publ. House, 1985, pp 91-101.
4. Goodman, J. W., "Introduction to Fourier Optics," New York: McGraw-Hill, 1968, pp 101-139.

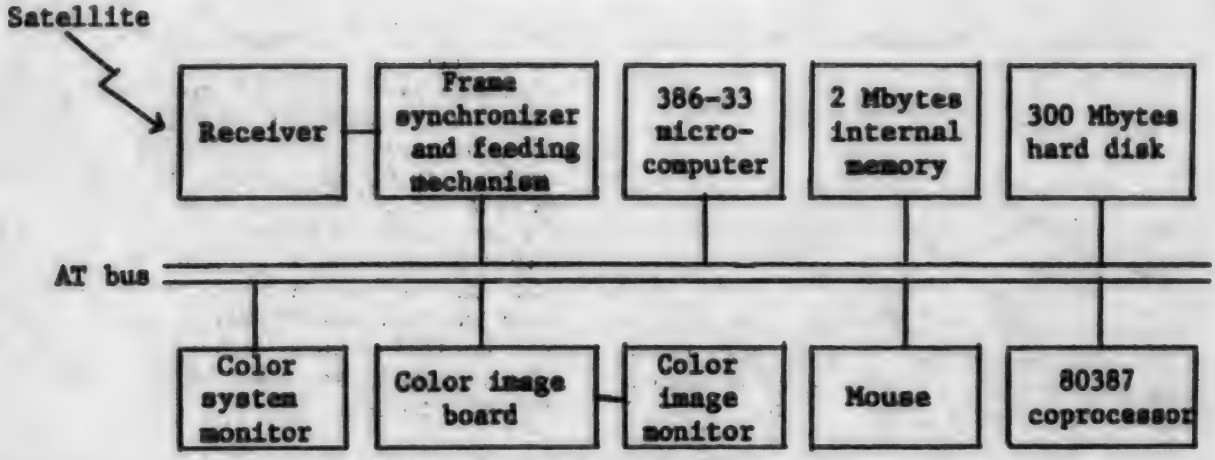

Figure 2. System Equipment

FTIR Magneto-Optical Spectrometer With High Optical Transmission Efficiency

94P60098B Shanghai HONGWAI YU HAOMIBO XUEBAO [JOURNAL OF INFRARED AND MILLIMETER WAVES] in Chinese Vol 12 No 4, Aug 93 pp 271-274

[Article by Liu Pulin [0491 2528 7207], Shi Guoliang [0670 0948 5328], et al. of the National Laboratory for Infrared Physics, Shanghai Institute of Technical Physics (SITP), CAS, Shanghai 200083: "FTIR Magneto-Optical Spectrometer With High Optical Transmission Efficiency"; MS received 20 Jan 93, revised 14 Jun 93]

[Abstract] An FTIR (Fourier transform infrared) magneto-optical spectrometer with high optical transmission efficiency has been developed from a novel design. The instrument's construction and characteristics are described, and test results including typical spectra are given. The system is based on a Brueker 113V FTIR spectrometer, with an operating spectral range of 10-10,000 cm^{-1} and a maximum resolution of 0.03 cm^{-1}. The liquid-helium Dewar/superconducting magnet system is an Oxford S11/12L-40-13, with a magnetic-cavity effective diameter of 40mm and a maximum field strength of 12 T. The five-reflector imaging system is independently developed. Overall system transmission efficiency is 0.37 (37 percent).

Figure 1, reproduced below, is a schematic diagram of the entire system, while Figures 2 and 3, not reproduced, show measured spectra for a test of the optical transmission system and photothermal ionization spectra (resolution = 0.15 cm^{-1}) of ultra-pure silicon under various magnetic fields. There are no tables.

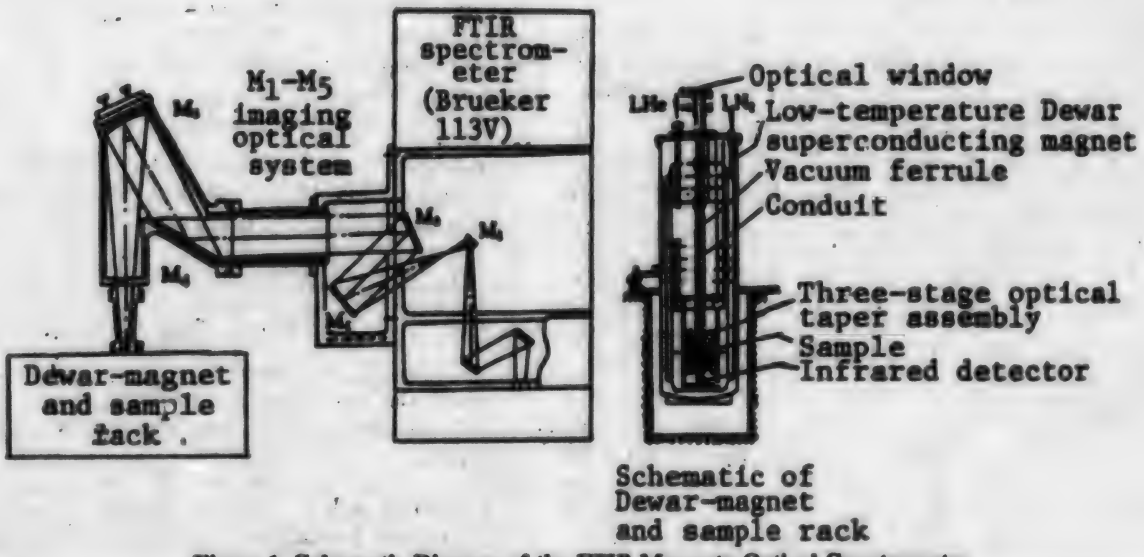

Figure 1. Schematic Diagram of the FTIR Magneto-Optical Spectrometer

References

1. McCombe, B. D., and Wagner, R. J., ADVANCES IN ELECTRONICS AND ELECTRON PHYSICS, 1974, 36:1.
2. Ibid., 1975, 37:1.
3. Kinch, M. A., Buss, D. D., J. PHYS. CHEM. SOL., 1971, 32:461.
4. Liu, W. J., Liu, P. L., et al., SPIE, 1991, 1519:415.
5. Zhu Jingbing, Liu Pulin, et al., BANDAOTI XUEBAO [CHINESE JOURNAL OF SEMICONDUCTORS], 1992, 13:729.
6. Ibid., p. 232.
7. Zhu, J. B., Liu, P. L., Liu, W. L., and Shen, S. C., SPIE, 1991, 1575:584.
8. Shen, S. C., SPIE, 1991, 1575:161.

Relation Between Thicknesses, Dielectric/Pyroelectric Properties of PVDF:TGS Composite Material Films

94P60098C Shanghai HONGWAI YU HAOMIBO XUEBAO [JOURNAL OF INFRARED AND MILLIMETER WAVES] in Chinese Vol 12 No 5, Oct 93 pp 397-403

[Article by Guo Guanjun [6753 0385 6511] of the Tank Academy, Physics Teaching & Research Section, Bengbu, Anhui 233013, Xu Pingmao [1776 1627 5399] of the Dept. of Optics, Shandong University, Jinan 250100, and Wang Min [3769 3046] of the Crystal Institute, Shandong University: "Relation Between Thicknesses, Dielectric/Pyroelectric Properties of PVDF:TGS Composite Material Films," supported by grant from NSFC; MS received 3 Jul 92, revised 10 Jun 93]

[Abstract] PVDF:TGS [polyvinylidene fluoride: triglycine sulfate] composite films of varying thickness have been developed. Experimental results show that the thinner the film is, the higher the dielectric constant, dielectric loss, and pyroelectric coefficient are. These experimental results are explained qualitatively. Room-temperature (15°C) detectors developed by the authors from these thin films (15-20 μm thick) have a detectivity D^* (500K, 12.5 Hz) of 1.55 x 10^8 cm-$Hz^{1/2}$-W^{-1}, an NEP [noise equivalent power] (500K, 12.5 Hz) of 1.95 x 10^{-9} W, and a photosensitive-area diameter of 2mm.

Four figures, not reproduced, show an SEM photo of the coarse surface of the composite film, a graph of dielectric constant vs. temperature, a graph of dielectric loss vs. temperature, and a graph of pyroelectric coefficient vs. temperature. There are no tables.

References

1. Skinner, D. P., Newnham, K. E., Cross, L. E., MAT. RES. BULL., 1978, 13:599.
2. Amin, M., Balloomal, L. S., Darwish, K. A., et al., FERROELECTRICS, 1988, 81:381.
3. Muralidhar, C., Pillai, P. K. C., J. MAT. SCI. LETT., 1987, 6:646.
4. Das-Gupta, D. K., Abdullah, M. J., J. MAT. SCI. LETT., 1988, 7:167.
5. Wang, M., Fang, C. S., Zhou, H. S., FERROELECTRICS, 1991, 118:191.
6. Sessler, G. M., "Electrets," New York: Springer-Verlag, 1980, p 120.

Optical Omega Network With Four-Function Optical Exchange-Switch for Digital Optical Switching Network

94P60110A Shanghai GUANGXUE XUEBAO [ACTA OPTICA SINICA] in Chinese Vol 13 No 12, Dec 93 pp 1105-1109

[Article by Cao Mingcui [2580 2494 5050], Luo Fengguang [5012 7364 0342], et al. of the National Laboratory of Laser Technology, Huazhong (Central China) University of Science & Technology, Wuhan 430074: "Four-Function Exchange-Switch Optical Omega Network for Digital Optical Switching Network," supported by grants from NDSTIC's Science Fund and NSFC; MS received 13 Oct 92, revised 25 Jan 93]

[Abstract] An optical Omega network with a four-function optical exchange-switch for a digital optical switching network is presented. The principle of the optical implementation of the four-function exchange-switch and Omega network via an 8-pixel liquid-crystal spatial light modulator (LCSLM) and special polarizing prisms is discussed in detail. The optical system and experimental results with twisted-nematic liquid crystal plates are given.

Figures 1, 3, 4, and 6, reproduced below, show an Omega interconnection network (P.S. = perfect shuffle, A-L are the twelve 2 x 2 switches), a schematic diagram of the optical Omega network with four-function optical exchange-switch (I and II are polarizing optical prisms, lines AB and CD indicate polarizing films, C_0 and C_4 are two of the eight pixels in the LCSLM, and PB_1 and PB_2 are prism blocks), the four states of the exchange-switch corresponding to the different states of the liquid-crystal pixels, and a schematic diagram of the optical Omega interconnection network with four-function optical exchange-switch arrays, respectively. Figures 2, 5, and 7, not reproduced, show a simple schematic of a four-function exchange switch, five

photographs (input light-beam permutation, left P.S. connection, right P.S. connection, down-spread connection, and up-spread connection) of the experimental results for the four-function optical exchange-switch, and five photographs of the experimental results for the optical Omega network with four-function optical exchange-switch, respectively. There are no tables.

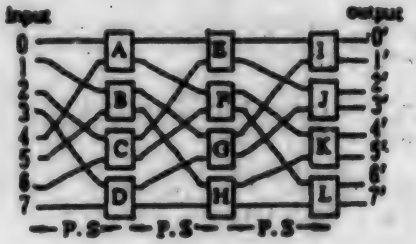

Figure 1. The Omega Interconnection Network (N = 8)

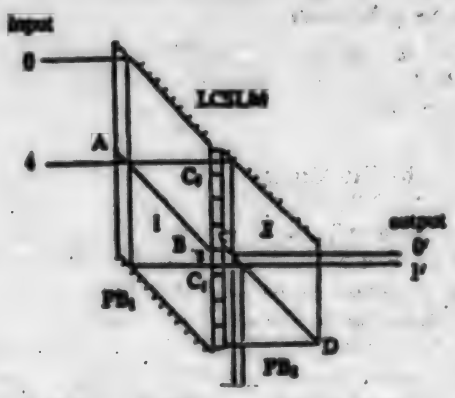

Figure 3. Schematic Diagram of Optical Omega Network With Four-Function Optical Exchange-Switch

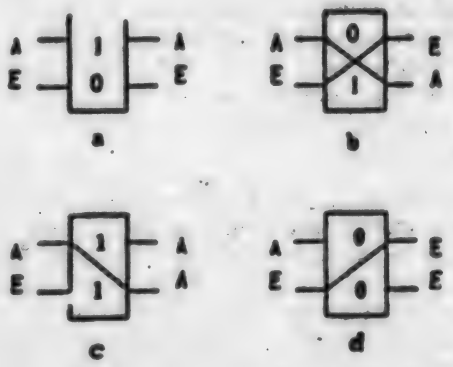

Figure 4. The Four States of the Exchange-Switch Corresponding to the Different States of Liquid Crystal Pixels

(a) the straight-through connection, (b) the exchange connection, (c) the down-spread connection, (d) the up-spread connection

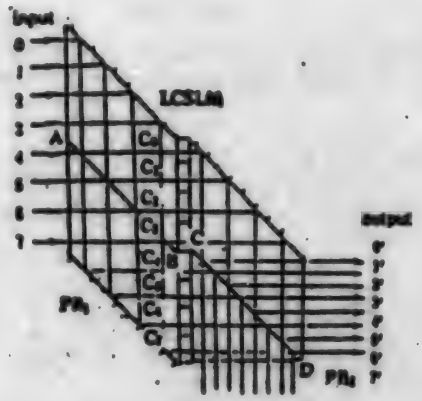

Figure 6. The Optical Omega Interconnection Network With Four-Function Optical Exchange-Switch Arrays

References

1. J. Jahns, M. J. Murdocca, "Crossover Networks and Their Optical Implementation," APPL. OPT., 1988, 27(15): 3155-3160.

2. Cao Mingcui, Li Hongpu, Liu Xiaan, et al., "Optical Hardware for the Perfect Shuffle Interconnection," OPTICAL COMPUTING AND PROCESSING, 1991, 1(1): 23-27.

3. Cao Mingcui, Luo Fengguang, Li Hongpu, et al., "Optical Perfect Shuffle-Exchange Interconnect Network Using Liquid Crystal Light Switch," APPL. OPT., 1992, 31: 6817-6819.

4. Cao Mingcui, Li Hongpu, Luo Fengguang, et al., "Optical Implementation of Perfect Shuffle/Exchange Omega Interconnection Network" [in Chinese], GUANGXUE XUEBAO [ACTA OPTICA SINICA], 1992, 12(12): 1129-1133 [translated in full in JPRS-CST-93-010, 27 May 93 pp 19-22].

5. K. H. Bremer, A. Huang, "Optical Implementation of Perfect-Shuffle Interconnection," APPL. OPT., 1988, 27(1): 135-137.

6. M. J. Murdocca, A. Huang, J. Jahns, et al., "Optical Design of Programmable Logic Arrays," APPL. OPT., 1988, 27(9): 1650-1660.

7. M. Murdocca, T. J. Cloonan, "Optical Design of a Digital Switch," APPL. OPT., 1989, 28(13): 2505-2517.

8. G. Eichmann, Yao Li, "Compact Optical Generalized Perfect Shuffle," APPL. OPT., 1987, 26(7): 1167-1169.

Shenzhen, Powerful Chips Base

40100033A Beijing CHINA DAILY (BUSINESS WEEKLY) in English 31 Jan 94 p 4

[Article by Zhang Xingbo: "Shenzhen, Powerful Chips Base" [cf. JPRS-CST-93-006, 6 Apr 93 p 41]]

[Text] Shenzhen—A Shenzhen-Hong Kong programme for producing super-large-scale integrated chips—the largest such programme in China—announced last week the establishment of its Chinese-side investment company.

The Shenzhen Saige High-Tech Investment Co., Ltd. will co-operate with a large European company in producing super-large-scale integrated chips in the Shenzhen Special Economic Zone and in conducting its after-processing work in Hong Kong.

The total investment is expected to exceed 8.7 billion yuan or $1 billion, according to Wang Dianpu, chairman of the board of the Shenzhen Saige Group, the major shareholder in the investment company.

At the opening ceremony last week, Wang noted that in 1991, the super-large-scale integrated programme was designated a State-class high-tech project.

After two years of preparation, the chairman said, the company was officially established with a total registered capital of 280 million yuan ($32 million).

The company has five shareholders. Besides the Saige group, they are the Shenzhen Urban Construction Group, Shenzhen New Industry Investment Co., Ltd., Shenzhen Zhongcheng Electronics Engineering Co., and Shenzhen Chang Ho Industry Co., Ltd., a joint venture by mainland and Hong Kong parties. The Saige group controls 62.6 per cent of all shares.

Wang said the company will invite more large companies in Shenzhen to buy shares.

In the near future, Wang said, the company will emphasize designing, producing, packaging, and testing technology for super-large-scale integrated circuitry and related industries.

Meanwhile, by making ample use of the State's preferential policies for the high-tech industry, Wang said, the company will develop new high-tech industries and diversify its business.

Over the long term, Wang said, the company hopes to develop into a powerful multinational corporation.

The super-large-scale integrated programme will be built in phases.

In the first phase, the company will build an after-processing plant and a design centre at the Futian Bonded Area in Shenzhen. It will cover more than 37,000 square metres.

According to Wang, the company will use advanced production equipment and technology to design, package and test various kinds of integrated circuitry.

The first-phase project, costing nearly $100 million, is expected to produce 318 million integrated chips each year. Most will be exported.

The project is expected to go into operation next year.

"It will be the most advanced in technology and the largest in scale of the country's competing manufacturers," Wang said.

He added that it would play an important role in promoting the country's electronics industry, narrowing the technological gap between China and developed countries, and pushing forward the industrial development in South China.

Further Reports on Fiber Optic Communications

Shanghai-Fujian Cable Operational

94P60109A Shanghai WEN HUI BAO in Chinese 2 Jan 94 p 2

[Article by Wang Shiyi [3769 0013 5030]: "Shanghai-Fujian Fiber Optic Cable Project Completed, Operational"]

[Summary] Ningbo, 1 Jan (WEN HUI BAO wire report)—The Shanghai-Fujian fiber optic cable, commissioned by the State Planning Commission, passed the acceptance check administered by MPT a few days ago here in Ningbo, Zhejiang Province, and is thus formally operational. This 1142.59-km-long cable project, which uses 24-core cable, runs from the Shanghai Long-Haul Telecommunications Tower through Hangzhou, Ningbo, Wenzhou, and Ningde, to the Fuzhou Telecommunications Hub Tower. Project final capacity will be 7 x 1920 circuits, while the now-completed phase provides 29,640 terminal circuits and 7860 repeater circuits.

First Cable TV Fiber Optic Trunk Line Transmission System

94P60109B Beijing RENMIN RIBAO OVERSEAS EDITION in Chinese 7 Jan 94 p 1

[Article by Hu Hongwei [5170 1347 0251] and Fang Ziyong [2455 5261 6978]: "Breakthrough for Nation's Cable TV Transmission Technology: Domestically Made Fiber Optic Trunk Line Transmission System Completed"]

[Summary] Hangzhou, 6 Jan (XINHUA)—The nation's first all-domestically-made cable TV fiber optic trunk line transmission system was recently completed. In the mid-to-late-80s, a number of developed nations announced perfection of such systems, while China's first imports and attempts to use this new high technology date from the early 90s. The now operational 10.35-km-long Xiangshan (Dancheng) to Qiangtouzhen [8259 7333 6966] transmission system incorporates domestically made devices and materials throughout. With installation and debugging completed, the system transmits clear, high-quality images.

Reports on Domestic Development of HDTV

In Search of Perfect TV

40100035A Beijing CHINA DAILY in English 14 Feb 94 p 5

[Article by staff reporter He Jun: "In Search of Perfect TV"]

[Text] Why not sharpen your TV—eliminate ghosts and noise and replace them with pure bright, beautiful pictures with natural colours and high-fidelity sound? Scientists around the world are in their final dash to replace the present TV sets in your home with magic boxes, called high-definition television (HDTV).

China, with most of its 800 million TV viewers still watching black-and-white, also has mapped out an ambitious plan, vowing to open its first experimental HDTV station by the turn of the century.

If what scientists predict comes true, this new generation of television will eliminate most of the shortcomings of the old set, including some things you may not have noticed.

As signals processed, transmitted and received are all digital, the loss of fidelity can be reduced to nothing theoretically or, at least, to an acceptable level, said Ma Changhua, technical adviser of the Ministry of Broadcasting, Film and Television.

The picture tube of HDTV will scan twice the number of lines current television can provide, so its fidelity can be as high as 35-millimetre film, said Ma, who is also in charge of the HDTV research project.

That means, when you stand at a distance of three times the screen height from the television, the picture is exactly the same as you can see at the real site, Ma added.

Therefore, the screen can be much larger than current ones. A common HDTV screen will be 32- or-36-inches.

It also changes the aspect ratio of the TV screen from the current 4:3 to 16:9, because a wide screen is much more comfortable on one's eyes.

As for your ears, the scientists have designed a so-called "5.1-channel sound system" to both comfort and shock viewers.

There are six different multi-directional sound channels.

Using digital technology, the new TV will be able to avoid most interference in the current television from both inside—signals in the same and adjacent channels—and outside—buildings, cars or vacuums.

Furthermore, with some technologies, one's home computer can also be linked to an HDTV monitor, greatly expanding the functions of the computer.

As TIME magazine reported, it can become an "interactive home information appliance" linked by fibre optics, made easy to use by software and driven by powerful computer chips.

The future of the multimedia industry, though not guaranteed, means the HDTV system may bring virtual reality into one's living room.

China

China's science circles are going all out to keep pace with the developed world on HDTV, which is advancing at a very rapid rate.

Japan is broadcasting an 8-hour HDTV programme each day through satellite. The U.S. is expected to open its first experimental HDTV station in 1996.

It is a must for China to develop HDTV technologies, said He Zuoxiu, an academician of the Chinese Academy of Sciences.

"The so-called HDTV issue is not only a matter of television, but also related to a wide range of other social questions," He said.

The technologies of digital processing, transmission, storage and display can be widely used in publications, medicine, the military, research, education, visual communication as well as other cultural and entertainment sectors, said the senior scientist.

With the great improvement in TV resolution, the movie industry in the future may not necessarily shoot a "film" with film, but tape, so that the cost can be greatly reduced, He said.

"China must master these technologies if it does not want to always follow others in the high-tech field," he said.

He also believes that the huge future HDTV market, both domestic and international, promises large profits.

An HDTV Strategy Research Group was organized in last April with authoritative scientists and officials from the State Science and Technology Commission (SSTC), the Chinese Academy of Sciences and China's top authorities in radio, film and television, the electronics industry, and post and telecommunications and the space industry.

According to the group's plan, now waiting for central government approval, China will post its HDTV system standards in 1997.

China so far has only a few computer-simulated HDTV systems in Ma Changhua's laboratory. These can display strikingly clear pictures.

China plans to establish a model HDTV system within two years. Scientists will actively prepare from now on the opening of the country's first experimental HDTV station around 2000, while developing its own HDTV industry.

The main task for China's HDTV development includes developing some key technologies and an industry to produce HDTV receivers, said Feng Jichun, an official with the State Science and Technology Commission (SSTC).

"This is the highest priority," he stressed.

China expects to start commercial production of HDTV receivers by the turn of the century, he said.

The United States plans to stop broadcasting its current common television in 15 years.

The process of replacing the current television system with a high definition one will be 5 to 10 years longer in China than in the U.S., according to the "most optimistic prediction" by Feng Jichun.

This is such a sophisticated project that it needs the close co-operation of all concerned government departments, industrial circles and research institutes, Feng said.

Technology

China is not capable of independently developing all the technologies related to HDTV, for which Japan, the European Community and the US have, or plan to, pour billions of dollars, Feng said.

The key HDTV technologies roughly can be classified as:

- Professional equipment, including cameras and recording and broadcasting equipment;
- 16:9 wide-screen monitors and receivers, especially picture tubes and the chips inside;
- Source encoding, compression and decoding;
- Transmission systems;
- Others.

Some technologies are still in the early research stage by scientists around the world. And none has so far been mastered by China.

"We will be seeking broad international co-operation," said the official.

The technology for the signal encoding, compression and decoding is one of the key fields the Chinese scientists are studying, he added.

China has focused sharply on the production of home-use HDTV receivers for they are comparatively easy to make as well as highly profitable.

Research on HDTV picture tubes has started in some electronics companies through co-operation with foreign firms.

Some scientists also have paid great attention to the design and manufacture of the special chips—the brain of digital HDTV.

Costs Remain Too High for China

40100035B Beijing CHINA DAILY in English 14 Feb 94 p 5

[Article by staff reporter He Jun: "Costs Remain Too High for China"]

[Text] While the world of high-definition television (HDTV), jointly created by the developed nations, is rapidly approaching, China has checked her pocketbook and doubts whether she can afford the technology before 2000.

A long debate among experts early last year concluded that an HDTV system is both affordable and profitable for China, especially in the economically stronger east and coastal regions—but not immediately.

Though most of China's 800 million TV viewers are still watching black-and-white sets, China's economic miracle in recent years promises that an increasing number of people will embrace the new technology, said Feng Jichun, an official with the State Science and Technology Commission (SSTC).

Chinese family incomes are expected to increase sharply in the next few years.

Meanwhile, production costs may reduce remarkably with technological improvement.

The retail price of an HDTV receiver was 4.5 million Japanese yen ($40,500) when it first hit the market in December 1990. And in May 1993 it was 980,000 Japanese yen ($8,820) for a 32-inch receiver with built-in decoder.

As American scientists develop a fully digital HDTV system, which is more advanced than the Japanese analogue one, the production cost of such HDTV receivers will drop to $1,000 by the turn of the century, according to some predictions.

Though the predictions seem over-optimistic, it is sure that the new technology will cost less.

But however promising the HDTV market, the investment needed to conquer it is too high to be acceptable for China.

Japan and European Community countries have poured a total of $3.5 to $4 billion into HDTV research in the last 20 years. The U.S. is also expected to pour billions of dollars into developing its digital technology.

Though China has focused on just a small part of the technological development, the scheduled research will still cost hundreds of millions of yuan, excluding that for industrial production of HDTV receivers, said Feng.

As the country has much more important fields crying for funds, the government can hardly spare much to make the TV screen more attractive, Feng added.

"My lab currently cannot even afford a complete set of HDTV hardware," said Ma Changhua, director of the SSTC's HDTV research project.

"But the research must go on," he continued. "If we stop, it will hand over a huge market to other countries and will cause a loss the country could hardly afford," he said.

China's national television network has 614 stations, covering 81.3 per cent of its nearly 1.2 billion population.

All the production, broadcasting and transmission equipment, plus the current 230 million TV sets and the TV set production lines, will be replaced by new ones for HDTV, he said, because so far HDTV is not compatible with the television now in use.

Theoretically, it is possible to broadcast the digital HDTV programmes on current TV sets, but it would produce low-quality pictures. HDTV receivers would perform much better, Ma said.

But all depends on the cost of technological development and the industrial production of such broadcasting facilities as well as the time it will take, he added.

With dramatic technological development in communications, especially in satellite broadcasting, China can hardly remain an isolated island of bad quality colour TV in a world of HDTV, he added.

In developed countries, industry plays the main role in HDTV development, but in China, both the government and the industry are short of cash.

There are also some "chicken-and-egg" problems for the promotion of HDTV, Zheng Zhihang, a researcher with the HDTV Research Institute of the Shanghai Jiaotong University, said at an HDTV seminar held last year in Beijing.

Consumers are unlikely to buy receivers until a wide variety of HDTV broadcasting is available; but broadcasters will hesitate to offer HDTV programmes until there are enough viewers to make it worthwhile.

Meanwhile, consumers are unlikely to buy receivers until the cost comes down to acceptable levels; but manufacturers can't bring the cost down until millions of consumers purchase HDTVs.

Nation Must Assess Situation

40100035C Beijing CHINA DAILY in English 14 Feb 94 p 5

[Article by staff reporter He Jun: "Nation Must Assess Situation and Choose an HDTV System"]

[Text] With China's growing determination to develop its own HDTV, the primary task ahead is to choose which hi-tech systems to emulate.

Since China is not technologically or financially capable of developing its own HDTV system, choosing the proper system is essential, said Feng Jichun of the State Science and Technology Commission (SSTC).

He said only one thing is certain now—China's HDTV will be a fully digital system.

In the last 20 years, developed countries have invested a lot of time and money in HDTV research. Currently, three systems are under development: the analogue systems of MUSE in Japan, HD-MAC in Europe and the full-digital system of America.

Although only a few years old, the U.S. full-digital HDTV system is now the most advanced and the future of the HDTV world.

Both Japan and Europe are devoting greater efforts to developing their own full-digital HDTV systems.

But developing HDTV in China is not as simple as copying another HDTV system. Different conditions in China must be met first, said Ma Changhua, director of the HDTV research project of SSTC.

Ma is also the former director and now the technical adviser of the Institute of Broadcasting Science of the Ministry of Broadcasting, Film and Television.

"It is not only a matter of adopting a set of new and advanced technologies for making television," Ma said. "We must consider all kinds of technical problems as well as the current status of the Chinese television."

A decision has to be made whether or not the current production lines of Chinese TVs are to be abandoned in favour of the better, clearer sets from the West, Ma added.

The world has three colour TV systems: NTSC in U.S., Japan and Asia, PAL in West Europe and China, and SECAM in East Europe and France.

Because of the "internal relations" between HDTV and current television, Ma said, it is possible to use present-day sets while replacing the conventional TV with HDTV.

But if China uses a system totally different from current televisions, all its TV station equipment and production lines may become obsolete.

Meanwhile, Ma said, there are many technical problems. For example:

Using the PAL system for its conventional TV, China's TV channel bandwidth is 8 megahertz (MHz).

If China uses the U.S. and Japan bandwidth of 6 MHz, which is likely to be used in the U.S. full-digital television, it is easier for programme exchange, but more difficult to re-allot the existing channels. So the country plans to use 8 MHz to get better picture quality.

But the difference among future HDTV systems will be smaller if all the countries adopt the full-digital style, Ma said.

By using digital technologies, television communications will be much easier in an HDTV world.

"I think the future HDTV sets can receive programmes from any country if a common standard is adopted," Ma said.

Though scientists dream of a world television system, the future HDTV is not likely to use a universal system.

For all the political and economic concern, the slogan "For the World Peace" that has appeared at so many international HDTV seminars is turning out to be wishful thinking.

Each country has to consider their own specific situations and make their own choice, Ma said.

Short-Wave Ray Tracing in Ionosphere

40100031C Beijing KONGJIAN KEXUE XUEBAO [CHINESE JOURNAL OF SPACE SCIENCE] in Chinese Vol 13 No 4, Oct 93 pp 306-312

[English abstract of article by Suo Yu-cheng of China Research Institute of Radiowave Propagation, Xinxiang 453003; MS received 24 Mar 92]

[Text] In accordance with the requirement of ground communications systems of remote distance for short-wave band, on the basis of the model calculation of the mean background of ionospheric parameters, a method is presented for calculating the trace of short-wave rays in the ionosphere. The work is mainly concentrated on two aspects. First of all, because the frequency of short waves is relatively higher, the magnetic and collision effects in refractive index are neglected, so that general ray equations are simplified. In the second place, a method of calculating the first-order partial derivative of ionospheric plasma parameters is presented. The calculation of the partial derivative is on the basis of model result of parameters of each ionospheric layer, that is, on the basis of mean background of ionospheric parameters.

This method can be used in HF communications system, and other short-wave systems such as target-position system of HF radar, etc.

China Joins World Leaders in Nuclear Physics

94FE0200B Beijing RENMIN RIBAO OVERSEAS EDITION in Chinese 29 Nov 93 p 3

[Article by Han Zhenjun [7281 2182 6511]]

[Text] Beijing, 27 November (Xin Hua)—Researchers at the Chinese Atomic Energy Research Institute had successfully built China's first radioactive nuclear secondary beam line on the largest domestic tandem accelerator. On 20 November, they succeeded in obtaining Carbon-11 and Fluorine-17 radioactive nuclear beams from the beam line. This achievement greatly expanded the scope and depth of nuclear physics research in this country; it also made China one of the world leaders in this field.

According to reports, researchers at the Tandem Accelerator National Laboratory used Boron-11 and Oxygen-16 produced by the accelerator to stabilize the nuclear beam, then used the newly constructed secondary beam line to separate, transport and focus the nuclear beams of different mass and energy; finally, the desired Carbon-11 and Fluorine-17 were obtained in the target chamber at the end of beam line. The test results indicate that the performance of this facility meets the expected performance indices. It is believed that currently only two or three large laboratories in the United States and Japan have constructed similar radioactive secondary facilities to carry out these experiments.

Today, the radioactive nuclear beam is an active area of research in nuclear physics. The knowledge base accumulated in nuclear physics has been built on the foundation of experimental research where more than 2,000 nuclides have been produced by bombarding a target with stable nuclear beams. But we have reached a point where it is very difficult to produce new nuclides using stable nuclear beams. Radioactive nuclear beam provides a possible means for producing thousands of yet undiscovered new nuclides; it also provides a unique opportunity for studying the evolution of celestial bodies, nuclear structures, and new phenomena and basic laws of nuclear reactions. As a consequence, the scope and depth of China's nuclear physics research will be significantly expanded.

This tandem accelerator has an end voltage of 13 million volts; it is located in the Tandem Accelerator National Laboratory of the Chinese Atomic Energy Research Institute. In the past, this accelerator has played an important role in China's nuclear physics research where it has been used to perform mass spectral analysis of beryllium-10, to simulate the single-particle effect in large integrated circuits, and to study the time of flight of abnormal fast neutrons.

This project is supported by the National Foundation of Natural Science and the Chinese Nuclear Science Foundation.

END OF FICHE

DATE FILMED

20 APR 1994